OPEN-FILE REPORT 22-09

Geochronology and Geomorphic Mapping to Estimate Debris-flow Depositional Ages and Recurrence Intervals Along State Highways 145 and 62, San Miguel County, Colorado

By Kassandra O. Lindsey and Lauren D. Broes

Colorado Geological Survey
Colorado School of Mines
Golden, Colorado

2022

Cover: Debris-flow deposits at Fan A and B impacting Colorado State Highways 62 and 145 in San Miguel County.
DOI: https://doi.org/10.58783/cgs.of2209.ugvy7542

Geochronology and Geomorphic Mapping to Estimate Debris-flow Depositional Ages and Recurrence Intervals Along State Highways 145 and 62, San Miguel County, Colorado

By Kassandra O. Lindsey and Lauren D. Broes

Matthew L. Morgan
DIRECTOR AND
STATE GEOLOGIST

TABLE OF CONTENTS

APPENDICES

LIST OF TABLES

LIST OF FIGURES

ACKNOWLEDGMENTS

The authors would like to thank the Colorado Department of Transportation (CDOT) for funding this project, and especially Ty Ortiz, formerly of the CDOT Geohazards program for his direction. The following individuals provided invaluable, expert internal and external reviews of this report: Matt Morgan (CGS Director and State Geologist), Kevin McCoy (BGC Engineering). Kimberly Cumella and Emiliano Lopez with the National Resources Conservation Service (NRCS) helped excavate soil pits and provided advice on soil development. Steve Forman (Baylor University) conducted the optically stimulated luminescence (OSL) age-dating analysis, contributed significant text discussing OSL dating methodology and statistical significance of the results. Beta Analytic (Miami, Florida) conducted carbon-14 age-dating analysis. Special thanks to U.S. Bureau of Land Management staff for granting land access and permission to dig soil pits.

CGS Geologist Lauren Broes excavating a soil pit at Fan A to collect samples for geochronological analysis.

1. SCOPE OF WORK

This project was developed in response to the request by Colorado Department of Transportation (CDOT) and San Miguel County for 1:24,000-scale mapping and geochronology of debris-flow deposits along State Highway 145 between Norwood and Telluride, and Highway 62 from the intersection of State Highways 52 and 145 to roughly halfway to Ridgway (**Figure 1**). Detailed mapping and age dating of debris-flow fans are helpful in hazard analysis and identification of sites where more intensive geotechnical investigations are necessary. These data can be used to estimate recurrence intervals, magnitude of events, and channel migration history. The results of this study are anticipated to be part of a larger effort to help San Miguel County develop a debris-flow early warning system by better understanding the history of debris-flow events in the canyons. The goals of this study included:

- Collect samples from exposed sedimentary layers within debris-flow deposits for age-dating analysis.
- Attempt to establish debris-flow recurrence intervals.
- Attempt to identify factors contributing to debris-flow initiation in the region.
- Compare results and feasibility of carbon-14 (^{14}C) and optically stimulated luminescence (OSL) age-dating techniques of debris-flow deposits.

The Colorado Geological Survey (CGS) identified two sites, based on accessibility and vegetation coverage, in San Miguel County, Colorado, for age dating (Figure 1). Fan A is located along State Highway 62, approximately 26 km west of Ridgway. Fan B is along State Highway 145, around 13 km southeast of Placerville.

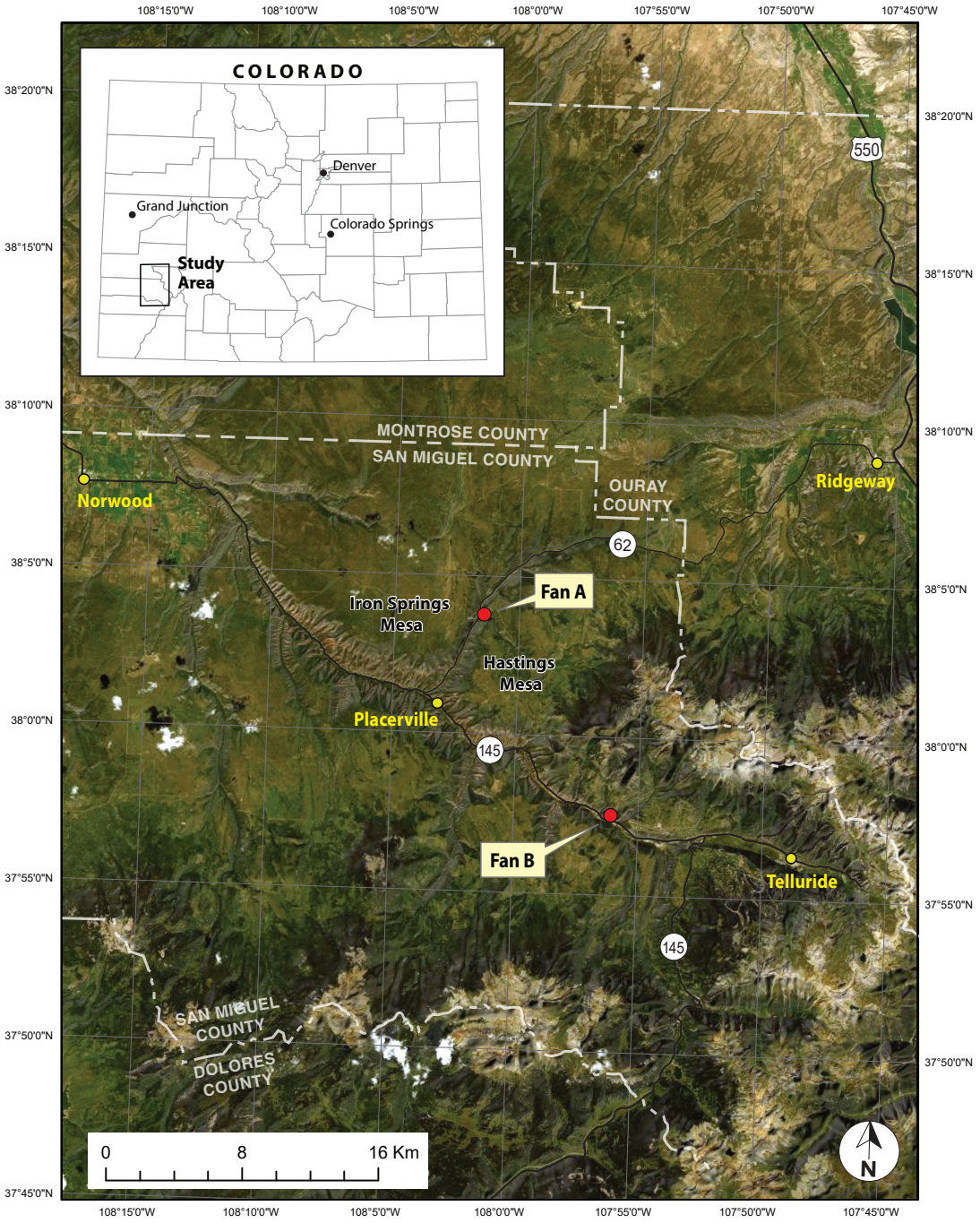

Figure 1. Location map of age-dating sites on debris-flow fans.

2. DESCRIPTION OF THE HAZARD

Debris flows, mudflows, and sediment-laden floods (herein referred to as debris flows) are common mass-wasting processes in the mountainous areas of Colorado. Debris flows, in combination with clear-water floods, pose significant hazards to communities, roads, railroads, and utilities in Colorado's mountain valleys and along range fronts. While debris flow and clear-water floods both typically affect valley bottoms and alluvial fans, debris flow pose a distinct hazard due to two important differences from clear-water floods:

1. Debris flows carry significant amounts of coarse sediment and debris in suspension (50% or greater sediment content by volume), whereas clear-water floods may carry floating debris and fine-grained, suspended sediment (as much as 10% sediment content by volume).

2. Debris flows tend to rapidly deposit their sediment and debris when channel gradients decrease (e.g., at road crossings or in developed areas), or when channel confinement is lost (Pierson, 2005).

Debris flow impacts on roads, railroads, and human-made structures may include serious injury or death, potentially costly repairs, and temporary or permanent road closures. Debris can block culverts and other hydraulic structures, leading to flooding and sediment deposition on the roadway or complete washout of the road. Where tributaries meet larger drainages, rapid deposition of sediment can occur and lead to upstream flooding and downstream water quality degradation.

Predicting debris flows can be difficult compared to other, similar hazards like clear-water floods. Establishing a recurrence interval for debris-flow events can help determine what factors contribute most to debris-flow initiation in an area. Age-dating debris flows and developing a record of historical events is important for establishing recurrence intervals.

3. PHYSIOGRAPHIC AND GEOLOGIC SETTING

3.1 Physiography

The study area lies within the northwestern San Juan Mountains along the boundary of the Colorado Plateau and the Southern Rocky Mountains physiographic provinces (**Figure 2**). Elevation ranges from 1,995 m to 3,761 m and the climate ranges from semi-arid to high alpine, depending on the elevation. Forest vegetation consists mainly of cedar, spruce, fir, and pine. Low temperatures average -16°C and highs average 24°C in Telluride, annually. Telluride averages 4.25 m of snowfall and 0.6 m of rain per year. The San Juan Mountains are affected by seasonal monsoons between July and September and much of the local rainfall occurs from pop-up thunderstorms, which may bring heavy downpours resulting in local flooding. Similar to variations in temperatures, there is a potential for higher snow averages at higher elevations.

3.2 General Geology

Fluvial erosion exposed the Triassic, Jurassic, and Cretaceous sedimentary rocks underlying valley walls and floor. The catchments above both fans are capped by the resistant Upper Cretaceous Dakota Sandstone which underlies most of the Hastings Mesa and Iron Springs Mesa (Figure 1, **Figure 3**, and **Figure 4**). This cliff-forming formation consists of two sandstone units separated by an interval of carbonaceous shale. The Brushy Basin and Salt Wash Sandstone members of the Jurassic Morrison Formation are slope- and ledge-forming sandstone, shale and siltstone unit as much as 250 m thick. Jurassic and Triassic formations underlie slopes at lower elevations in the valley. The Jurassic Wanakah Formation grades from a limy siltstone with thin limy sandstones at the top, to a soft, fine-grained sandstone (Bilk Creek Sandstone) in the middle, and bituminous limestone (Pony Express

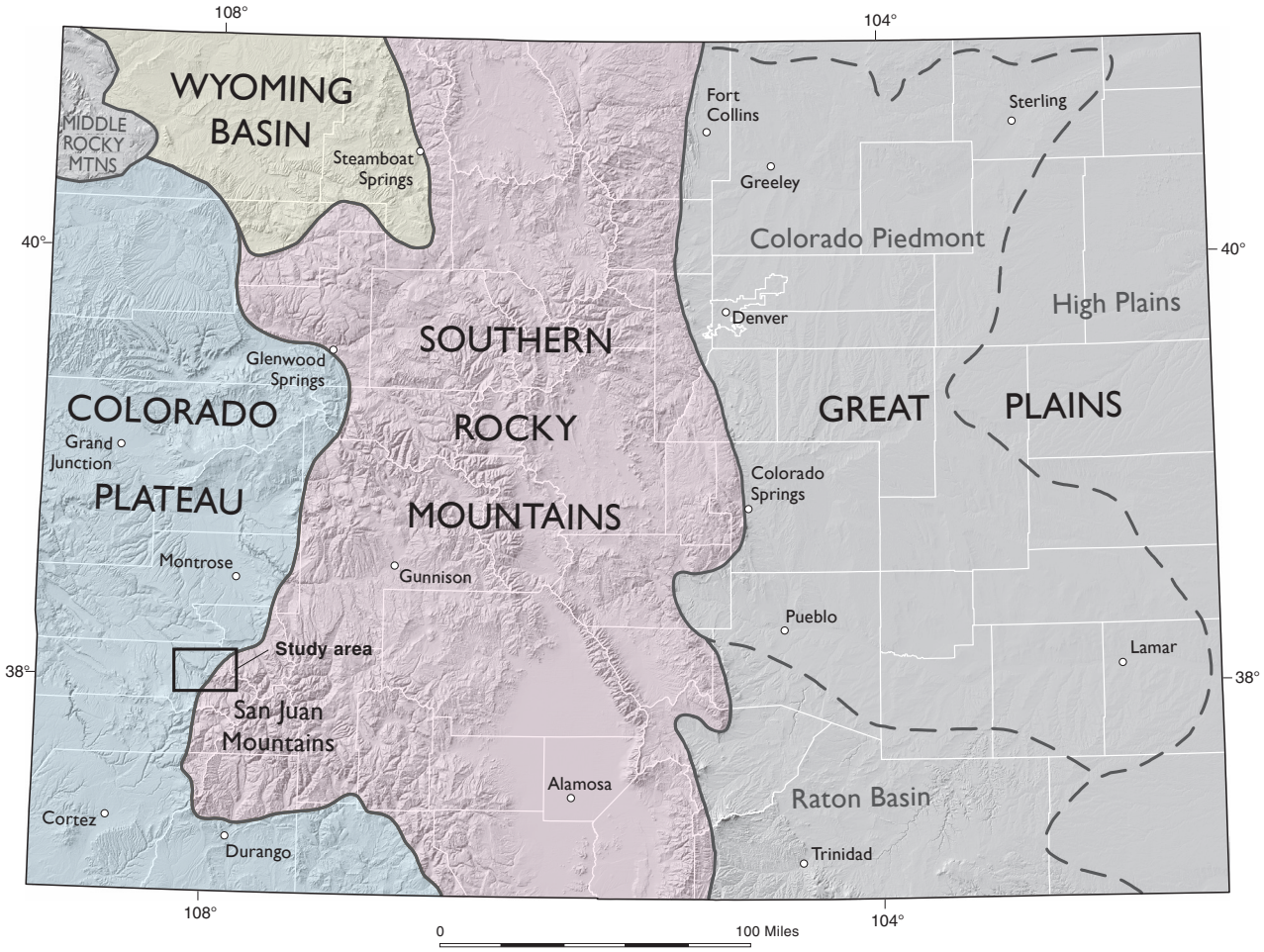

Figure 2. Physiographic province map of Colorado. The study area (bold black box) is located on the Southern Rocky Mountain border with the Colorado Plateau.

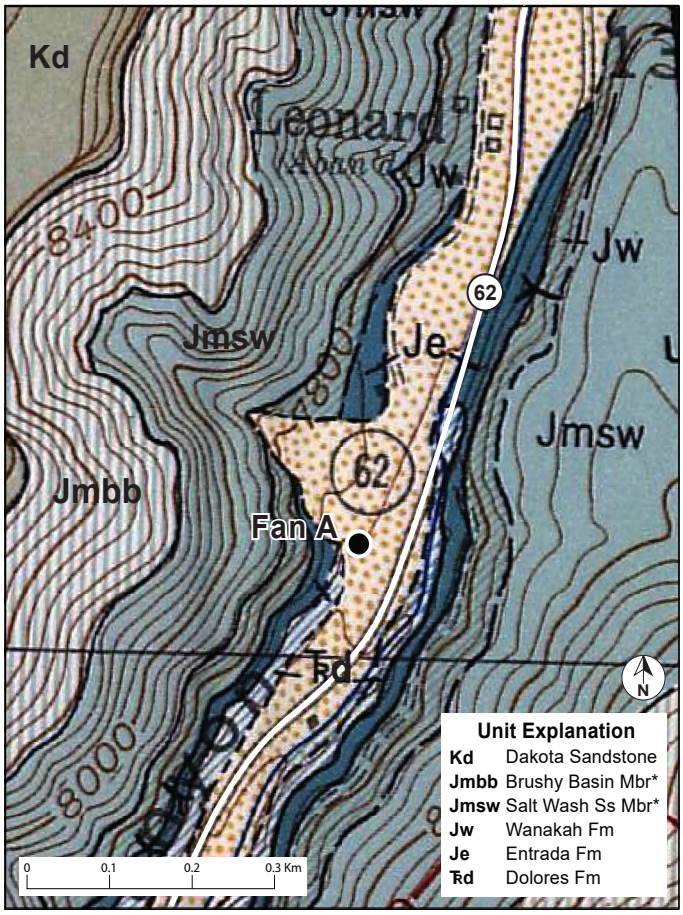

Figure 3. Geology of Fan A and surrounding area from the 1:24,000-scale Placerville areal geologic map by Bush and others (1959). Mapping indicates Dakota Sandstone, the Brushy Basin and Salt Wash members of the Morrison Formation, and Wanakah Formation as potential source area units for debris flows at Fan A. Debris-flow deposits mantle portions of the Wanakah, Entrada, and Dolores formations at the site.

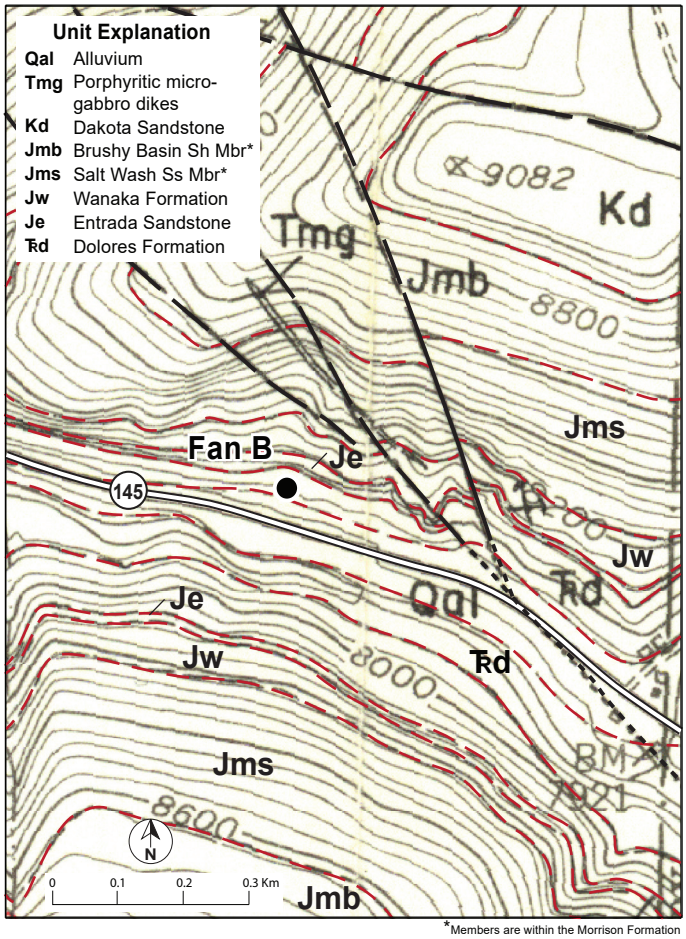

Figure 4. Geology of Fan B and surrounding area from the 1:24,000-scale Gray Head reconnaissance geologic map by Bush and others (1961). Mapping indicates Dakota Sandstone, the Brushy Basin and Salt Wash members of the Morrison Formation, and Wanakah Formation as potential source area units for debris flows at Fan B. Faults are mapped and gabbro dikes outcrop above the fan as well. Debris-flow deposits mantle portions of the Wanakah, Entrada, and Dolores formations at the site.

limestone) at the base. The unit underlies slopes above the valley floor. The Jurassic Entrada Sandstone, which is comprised of mudstones, siltstones, and sandstones, underlies the Wanakah Formation and portions of the valley floor. The lowermost exposed unit in the valley is the Triassic Dolores Formation. This unit is comprised of siltstone, sandstone, shale, and beds of limestone-pebble conglomerates. The Vanadium fault, three mapped north-west trending faults, and an igneous dike that parallels the faults, cross-cut the catchment above Fan B (Bush and others, 1961; Figure 4). The faults were likely active during the Laramide orogeny (~40-70 million years ago; Bush and others, 1959).

The Dakota Sandstone supplies many of the boulders that line the margins of the current active (youngest) channel at the sites. The probable debris-flow initiation zone(s) are underlain by colluvial soils developed on the Brushy Basin Member of the Jurassic Morrison Formation in the upper catchment (Figure 3 and Figure 4). The Morrison Formation is capable of supplying significant quantities of sediment to a debris flow. The Jurassic Wanakah Formation, Entrada Sandstone, and Triassic Dolores Formation may contribute sediment, depending on debris-flow runout (Figure 3). Faults and dikes above Fan B are unlikely to have increased the frequency of debris flows through seismic activity during the Quaternary. However, in conjunction with the igneous intrusion, local faulting could influence water flow pathways and indirectly affect slope stability above Fan B.

During the Late Pleistocene (126,000 – 11,700 years BP), a 5,000 km^2 ice cap covered the San Juan Mountains at the local last glacial maximum (~23,500 – 21,000 years BP) during the Pinedale Glaciation (**Figure 5a**) (summarized in Leonard and others, 2017; Schweinsberg and others, 2020). Broad ice fields covered the region and large valley glaciers spread in all directions except the west (Carrara, 2011; Benson and others, 2005). The largest glacier in the region, the Animas

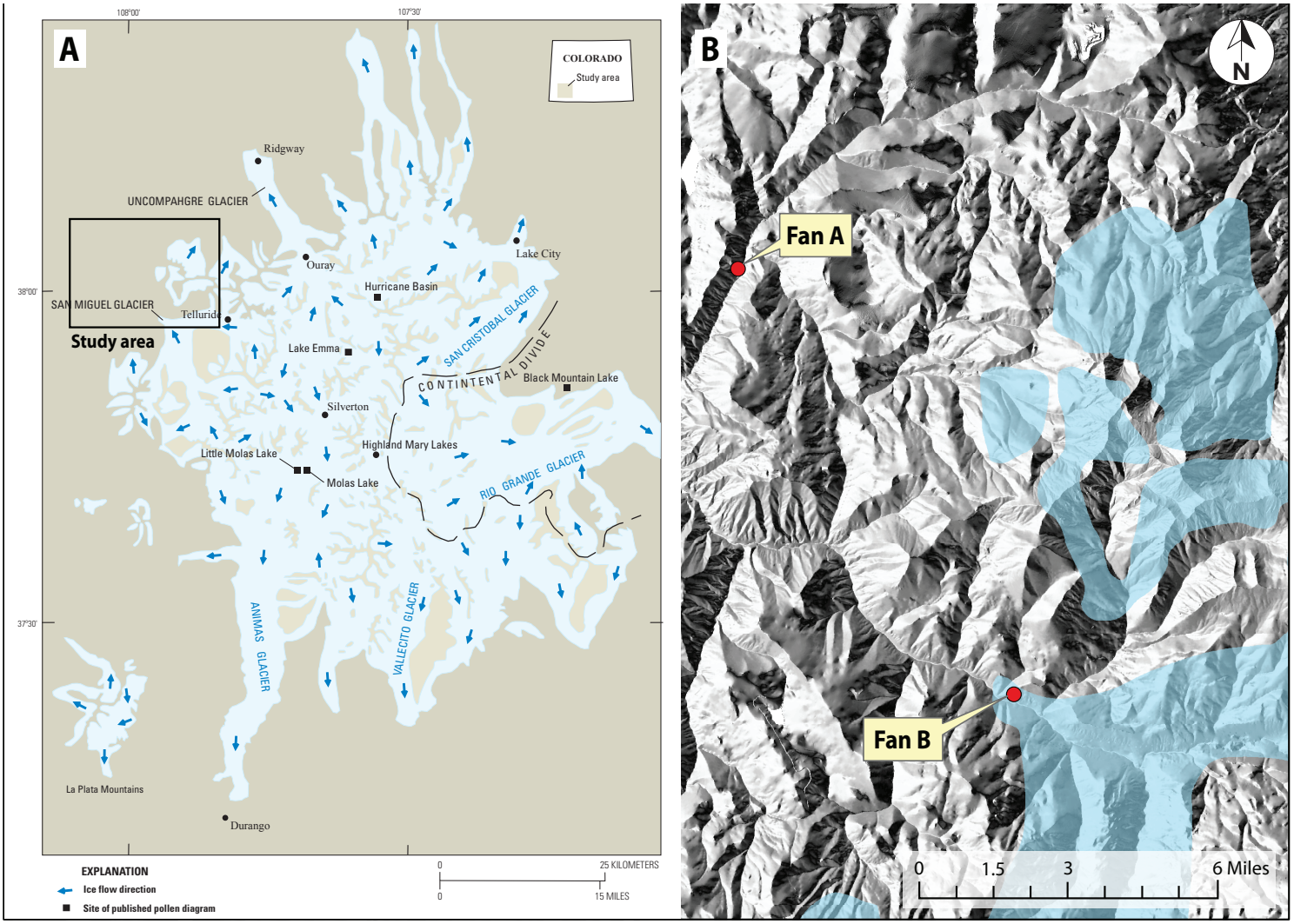

Figure 5. (a) Figure from Carrara (2011) illustrating glacial extents in the region during the Pinedale Glaciation with the approximate study area location shown with a black box, and (b) The San Miguel Glacier's extent during the Pinedale Glaciation in the study area (modified from Carrara, 2011 and Atwood and Mather, 1932.) Fan A is outside the glaciated zone. Fan B is located inside the maximum extent of glaciation.

Glacier, lay south of the study area and filled the Animas River valley to present-day Durango (Attwood and Mather, 1932). The Uncompahgre Glacier occupied the Uncompahgre River valley, to the east of the study area, and extended beyond present-day Ridgway (Atwood and Mather, 1932).

Glacial retreat in this region commenced earlier than other areas in Colorado, around 21,000 to 19,400 years BP (Leonard and others, 2017; Schweinsberg and others, 2020; Guido and others, 2007). Additionally, glaciers retreated faster, although constantly likely due to a regional increase in temperature concurrent with a decrease in precipitation (Leonard and others, 2017; Schweinsberg and others, 2020; Guido and others, 2007). The Pinedale Glaciation culminated around 14,000 to 12,300 years BP in the San Juan Mountains (Leonard and others, 2017; Ward and others, 2009; Guido and others, 2007). Glaciers likely did not extend as far as Fan A, though perennial ice sheets may have been present during exceptionally cold years during the Pinedale Glaciation (**Figure 5b**).

4. METHODS

4.1 Optically Stimulated Luminescence and Carbon-14 Sampling of Debris Flows

This study is intended, in part, to serve as a pilot project for testing the feasibility of OSL dating methods on debris-flow deposits in Colorado. Dr. Steven Forman, head of the Geoluminescence Dating Research Laboratory at Baylor University, provided a thorough explanation of OSL analysis that is included in **Appendix A**. In short, when quartz or feldspar grains are eroded from bedrock or a deposit, exposure to sunlight results in complete or partial luminescence resetting for those grains. Optically stimulated luminescence analysis methods can then estimate the time of burial for the quartz or feldspar grains. These methods are most commonly used to estimate the time of burial for fluvial or eolian sediments because those depositional environments most often result in complete solar resetting. Optically stimulated luminescence samples are collected by hammering a stainless-steel tube horizontally into a freshly cleaned vertical section of sediment. Stainless-steel tubes are necessary to shield the sample from any potential solar resetting at the time of sampling. Moderately to well-sorted, quartz- or feldspar-rich sand lenses are the most ideal samples for OSL analysis. Samples at both ends of the tube are removed prior to analysis in order to eliminate any grains that may have been exposed to the sun during sampling.

Beta Analytic performed Accelerator Mass Spectrometry (AMS) analysis for all submitted ^{14}C samples. Ten grams of sediment or more was submitted for each sample. A more detailed description of analysis methods can be found at the Beta Analytic web page. In short, sediment samples are first dried with methanol or dry ice. Carbon from the sediment samples is obtained from combustion at >800°C under 100% oxygen atmosphere and AMS measurements are performed on graphite produced by hydrogen reduction of the carbon sample over a cobalt catalyst. Results are obtained by measuring ^{14}C relative to ^{14}C in Oxalic Acid II in one of Beta Analytic's particle accelerators. When solid organic material is present, it is converted to CO_2 with an elemental analyzer and an isotope-ratio mass spectrometer calculates carbon. Conventional Radiocarbon Ages returned by the samples are then converted to calendar years.

4.2 Mapping and Fan Selection

Fan A and Fan B were selected because they were located on public lands, interpreted as likely to contain nearly complete sediment records of the most-recent events, and were easily accessible with sampling equipment. Furthermore, they were located along the CDOT corridor where future debris-flow events have the potential to impact the road. At this location, there are existing exposures of the fan stratigraphy that provided an opportunity to closely examine and potentially age-date a succession of debris-flow events. For both sites, geomorphic maps were created in ArcGIS using hillshaded 1-m resolution lidar imagery (Quantum Spatial, 2018). Multiple debris-flow fans were delineated on the basis of visually interpreted surface roughness depicted on lidar imagery **(Figure 6** and **Figure 8)**. The maps were used to identify lobes with the highest anticipated potential to estimate different ages **(Figure 7** and **Figure 9)**. One ^{14}C and one OSL sample was collected from exposed debris-flow units underlying each lobe. Deposits were sampled to establish approximate deposit age and estimate recurrence interval. Photography and logging for each sample site is presented in **Appendix B**.

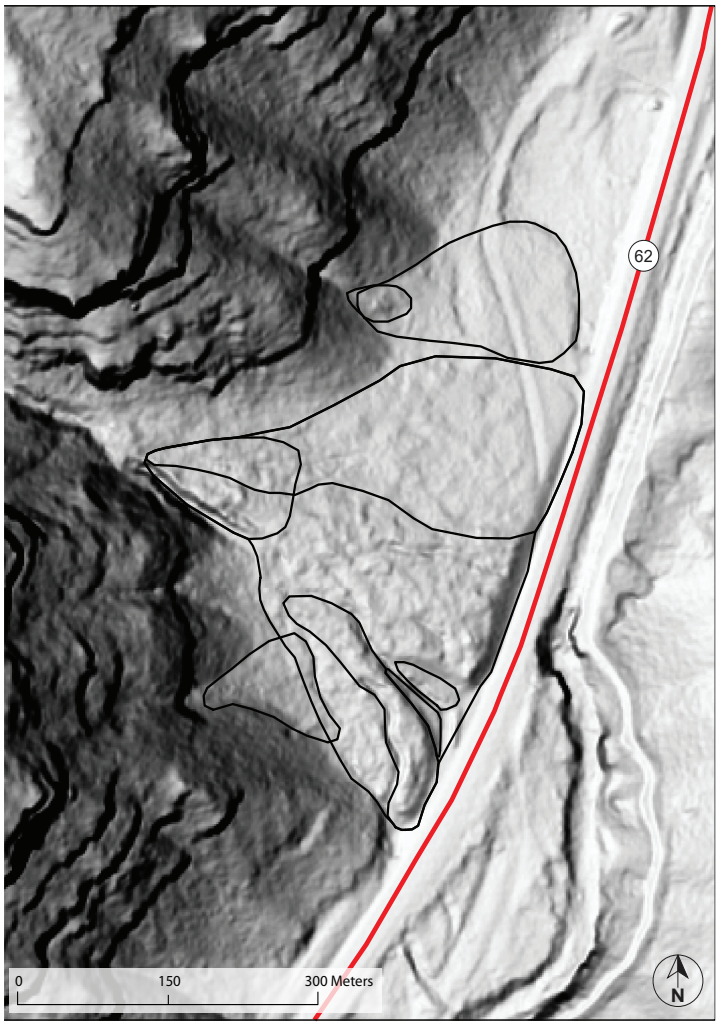

Figure 6. Geomorphic mapping of debris-flow lobes at Fan A. Nine were identified using 1-m resolution lidar (Quantum Spatial, 2018) based on apparent surface roughness.

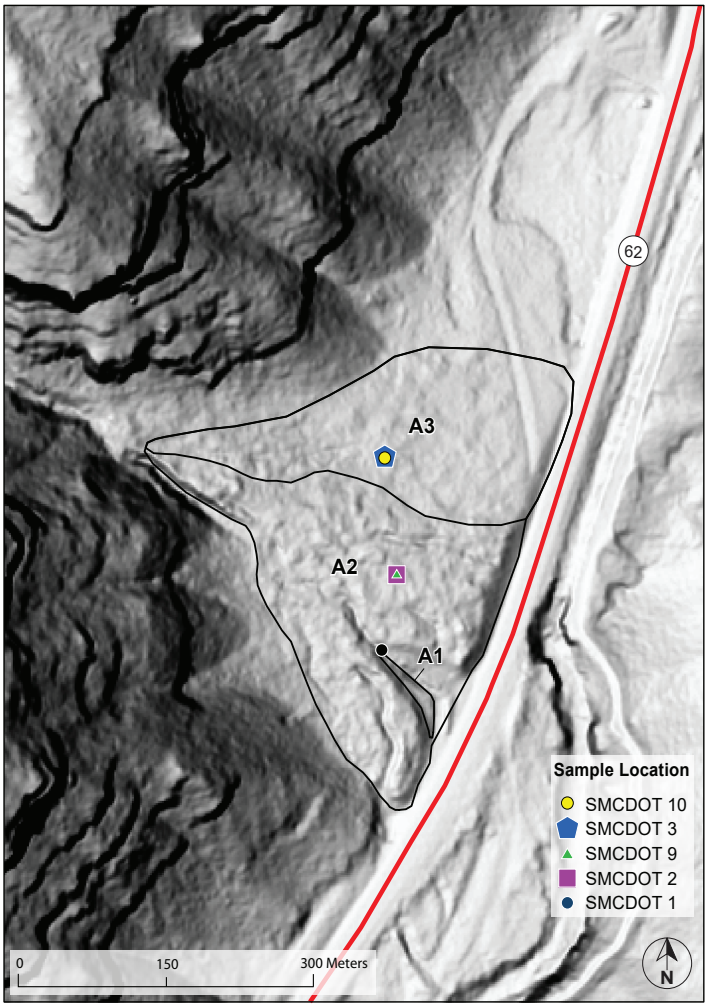

Figure 7. Hillshaded 1-m resolution lidar annotated with separate debris-flow events (A1, A2, A3) delineated based on surface roughness. Sample sites were identified to estimate the ages of mapped lobes across the fan surface.

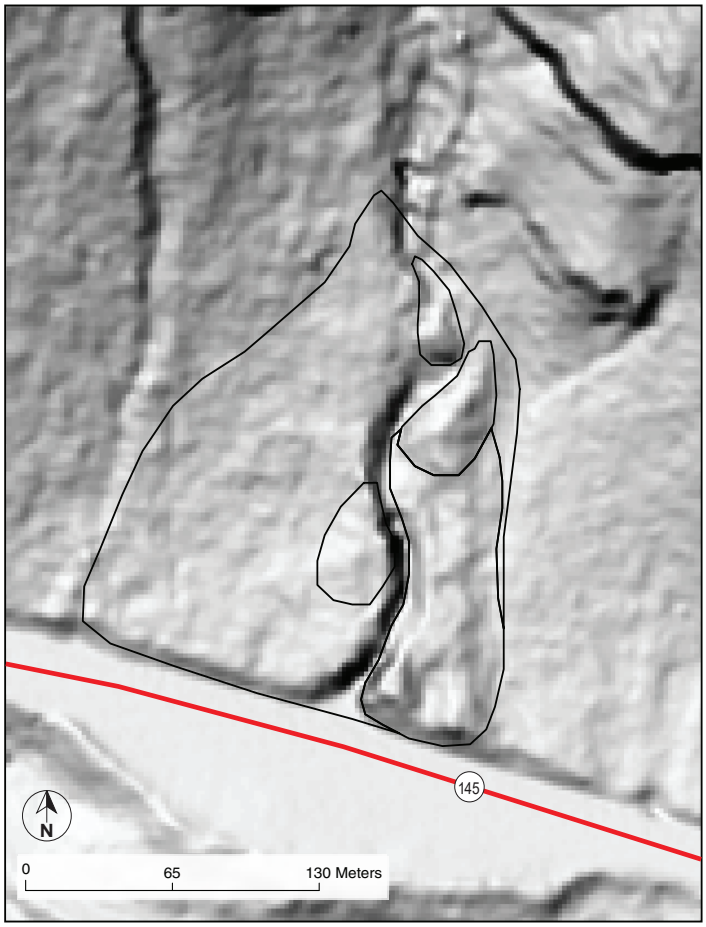

Figure 8. Geomorphic mapping of debris-flow lobes at Fan B. Five were identified using 1-m resolution lidar (Quantum Spatial, 2018) based on apparent surface roughness.

4.3 Fan A

Nine individual lobes were delineated using lidar imagery (Figure 6). Three of the lobes (A1, A2, and A3) were sampled to estimate the age of events across the fan surface (Figure 7). Lobes A1, A2, and A3 are located on public lands. To estimate the age of lobe A1, two samples were collected from a vertical face, approximately 1.5 m high, exposed by the modern channel. Detailed sample photography (**Figures B1-B3**) and logging is presented in Appendix A.

Sample SMCDOT 1 was collected from sandy sediment between gravel clasts in "unit 3" (Figure B1), the lowermost debris-flow deposit naturally exposed in the incised channel, approximately 1.5 m below ground surface (bgs). Sample SMCDOT 8 was collected from pebbly sand in "unit 2" (Figure B1), the uppermost debris-flow unit, approximately 40 cm bgs.

A soil pit, located approximately 35 m north of SMCDOT 1 and 8 on lobe A2, was hand dug to approximately 1 m in depth to expose debris-flow units. Samples SMCDOT 2 and SMCDOT 9 were collected from two different units exposed at this location (Figure B2). Sample SMCDOT 2 was collected from sandy sediment between gravel clasts in "unit 2", the lowermost debris-flow unit exposed at this site, approximately 76 cm bgs. Sample SMCDOT 9 was collected from clayey sand in the uppermost unit ("unit 1") exposed at this location, approximately 15 cm bgs.

A second soil pit, located approximately 62 m north of SMCDOT 2 and 9 on lobe A3, was hand dug to approximately 90 cm. Samples SMCDOT 3 and 10 were collected from two different units exposed at this location (Figure B3). Sample SMCDOT 3 was collected from a clayey sand in the lowermost exposed unit, "unit 2", approximately 70 m bgs. Sample SMCDOT 10 was collected from sandy sediment between gravel clasts in the uppermost unit, "unit 1", approximately 40 cm bgs. Twelve samples in total were collected from Fan A; six for ^{14}C analysis and six for OSL analysis.

4.4 Fan B

Five individual lobes were mapped on the basis of apparent surface roughness on lidar imagery and relative position in the landscape (Figure 8). An active channel separates two

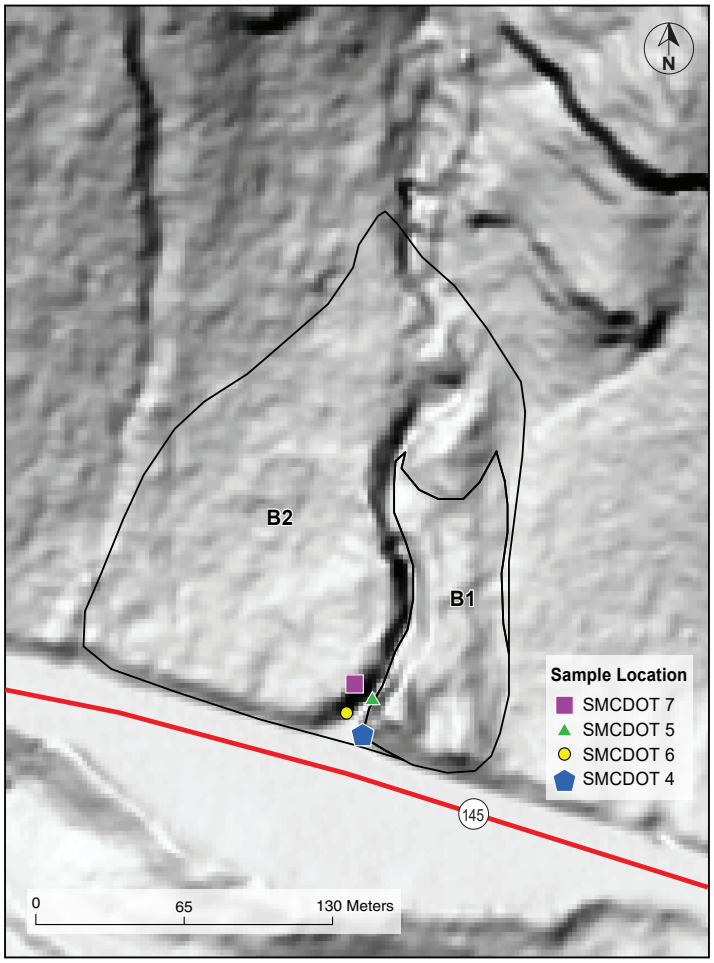

Figure 9. Initial debris flow lobe mapping and sampling locations at Fan B.

lobes (B1 and B2) and exposes a series of three or four individual debris-flow deposits (Figure 9). Four sets of ^{14}C and OSL samples were collected (Figure 9). Detailed sample photography (**Figure B4-B7**) and logging is presented in Appendix A.

At least four separate units are visible in an exposure of lobe B2, on the west side of the channel at Fan B. Sample SMCDOT 4 was collected from sandy sediment between gravel clasts in "unit 3", approximately 4.6 m bgs (Figure B4). At this location, "unit 1" and "unit 2" were not accessible from the road or channel and "unit 4" was almost entirely covered with colluvium. Therefore, sample SMCDOT 5 was collected approximately 12 m north of SMCDOT 4, from "unit 2" (Figure B5). Sample SMCDOT 5 was collected from sand in "unit 2", approximately 3.5 m bgs. The first sampling attempt was in loose sediment mantling the exposure and therefore it was resampled directly below.

An additional four debris-flow deposits are exposed on lobe B1 on the east side of the channel. Sample SMCDOT 6 was collected from sandy sediment between clasts in "unit 4", approximately 5.8 m bgs (Figure B6). At this location, "unit 1" and "unit 2" were not accessible from the road or channel, and "unit 3" was not sampled due to budget constraints. Sample SMCDOT 7 was collected approximately 6 m north of SMCDOT 6. Stratigraphy at SMCDOT 7 is difficult to discern in Figure B7 because the channel walls are steep and mostly covered by colluvium. Sample SMCDOT 7 was collected from sandy sediment between gravel clasts from a unit correlative with "unit 2" in Figure A6. We collected a total of four ^{14}C and four OSL samples from Fan B.

5. ANALYSIS AND RESULTS

5.1 Carbon-14 and Optically Stimulated Luminescence

A summary table of age-dating results is presented in **Table 1**. Full summary tables are in **Appendix C**. Ten samples were submitted for bulk carbon analysis and nine returned ages within detectable range. The full summary table of these results is presented in Appendix C, **Table C1**. Three samples were submitted for OSL analysis; one sample from Fan A and two samples from Fan B for OSL analysis (Table 1) and results from the OSL analysis are summarized in Appendix C, **Table C2**. Single aliquot regeneration (SAR) protocols (Murray and Wintle, 2003; Wintle and Murray, 2006) were used to estimate the apparent equivalent dose of the 250-150 or 100-63 μm quartz fraction, depending on which size fraction yielded at least 0.50 g for 41 to 36 separate aliquots **(Figure 10)**. The SAR protocols resolved equivalent doses of the samples. Thirty-five to fifty-two quartz aliquots were used to calculate the statistical significance of the equivalent dose population (Figure 10). The equivalent dose (D_e) distributions were log-normal and exhibited a range of overdispersion values (Figure 10).

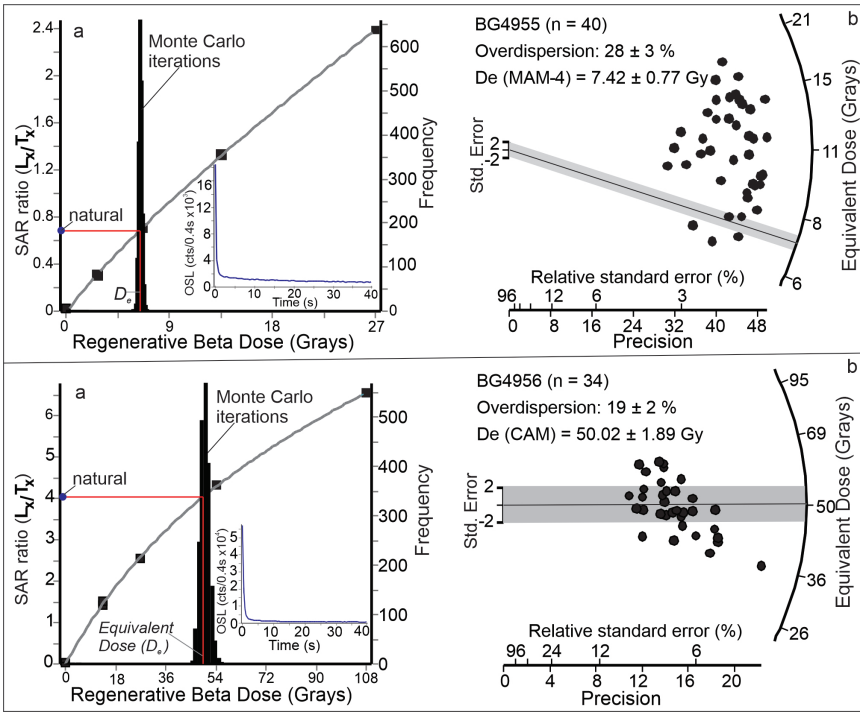

Figure 10. (a) Representative regenerative dose growth curves, with inset representative natural shine down curves, and (b) radial plots of equivalent dose values on small aliquots. Sample SMCDOT 3 yielded a 23 ± 3% overdispersion and the minimum age model (MAM) confined the age estimate to 1,985 ± 210 yrs BP. Sample SMCDOT 6 yielded a 19 ± 2% overdispersion and the central age model (CAM) confined the age estimate to 14,910 ± 720.

Bulk ^{14}C analysis was conducted for all the samples except SMCDOT 8. Sample SMCDOT 8 yielded an age estimate beyond detection (>43,500 cal yrs BP) for ^{14}C, likely due to contamination by Cretaceous-age coal. Results from the ^{14}C analysis is described in the Discussion (section 6).

Table 1. Summary table of age-dating estimates analyzed by ^{14}C and OSL analysis methods. Three samples were analyzed with both methods: SMCDOT 3, 4, and 6.

Field Number	^{14}C Age (cal yr BP)	OSL Age (SAR-OSL)
SMCDOT 1	28,011 – 27,660	-
SMCDOT 2	25,051 – 24,425	-
SMCDOT 3	12,819 – 12,707	1,985 ± 210
SMCDOT 4	5,468 – 5,314	12,312 ± 530
SMCDOT 5	3,271 – 3,140	-
SMCDOT 6	4,150 – 3,973	14,910 ± 720
SMCDOT 7	1,344 – 1,270	-
SMCDOT 9	16,905 – 16,432	-
SMCDOT 10	9,037 – 8,971	-

5.2 Fan A

Age estimates yielded from the ^{14}C sample results indicate a north-trending depositional pattern across Fan A, starting at SMCDOT 1 **(Figure 11** and **Table 2)**. Mean recurrence interval of the pre-historic events at this site, 3,766.3 years, was calculated by dividing the period of record returned by ^{14}C samples by the number of events (Crovelli, 2000): 18,831.5 (years between SMCDOT 1 and 10) divided by 5.

Table 2. Summary of age estimate yielded by bulk carbon analysis. Ages are self-consistent and may indicate a progression of deposition across the fan from south to north.

Sample Number	^{14}C Age (cal yr BP)	Elevation (m)
SMCDOT 10	9,037 to 8,971	2,368.4
SMCDOT 3	12,819 to 12,707	2,368.1
SMCDOT 9	16,905 to 16,432	2,367.1
SMCDOT 2	25,051 to 24,425	2,366.4
SMCDOT 1	28,011 to 27,660	2,360.2

The OSL sample collected at SMCDOT 3 yielded an age estimate of 1,985 ± 210 yrs BP, which is significantly younger than the correlating ^{14}C sample (12,819 to 12,707 cal yrs BP; Table 1). The overdispersion for the analyzed quartz grains in the OSL sample is 28 ± 3% (Figure 10; Table C2). While this is over the threshold (25%) for indicating a single-age population, the minimum-age model (MAM) indicates the 1,985 ± 210 yr BP age is still statistically significant and accurate. The sample was collected within 1 m of the ground surface, which could account for the higher overdispersion compared to the other samples (discussed more in Chapter 6).

5.3 Fan B

The ages yielded from the ^{14}C samples at Fan B indicate lateral fan migration across the area since the ages alternate on either side of the recent channel **(Figure 12; Table 3)**. Mean recurrence interval of 1,021 years was calculated by dividing the period of record returned by ^{14}C samples by the number of events (Crovelli, 2000): 4,084 (years between SMCDOT 4 and 7) divided by 4.

Samples SMCDOT 4 and 6 (OSL) yielded age estimates of 12,312 ± 530 and 14,910 ± 720 yrs BP, respectively. Overdispersion calculated for SMCDOT 4 and SMCDOT 6 is 13 ± 2% and 19 ± 2%, respectively, indicating single age populations in the quartz grains analyzed for both samples (Figure 10; Table C2). The results also indicate the samples yielded statistically significant ages. The corresponding ^{14}C samples are considerably younger than the ages reported by OSL analysis (Table 1). Both methods were self-consistent, yielding age estimates within a few thousand years of each other. However, ^{14}C and OSL sets differed from each other.

Table 3. Summary of ages yielded by ^{14}C. Ages may indicate lateral fan migration.

Sample Number	^{14}C Age (cal yr BP)	Elevation (m)
SMCDOT 7	1,344 – 1,270	2,421.6
SMCDOT 5	3,271 – 3,140	2,418.9
SMCDOT 6	4,150 – 3,973	2,416.5
SMCDOT 4	5,468 – 5,314	2,417.4

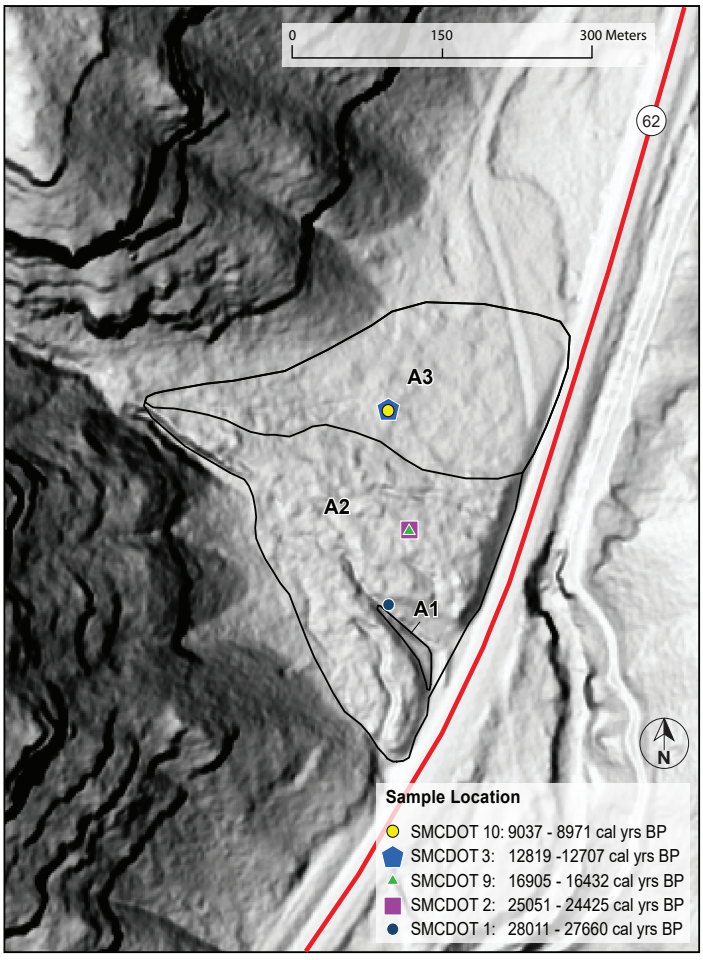

Figure 11. Distribution of ^{14}C age estimates at Fan A. Ages indicate a steady progression of deposition starting at the southernmost sample location, advancing to the northernmost sample location. Age estimates are consistent with apparent surface roughness.

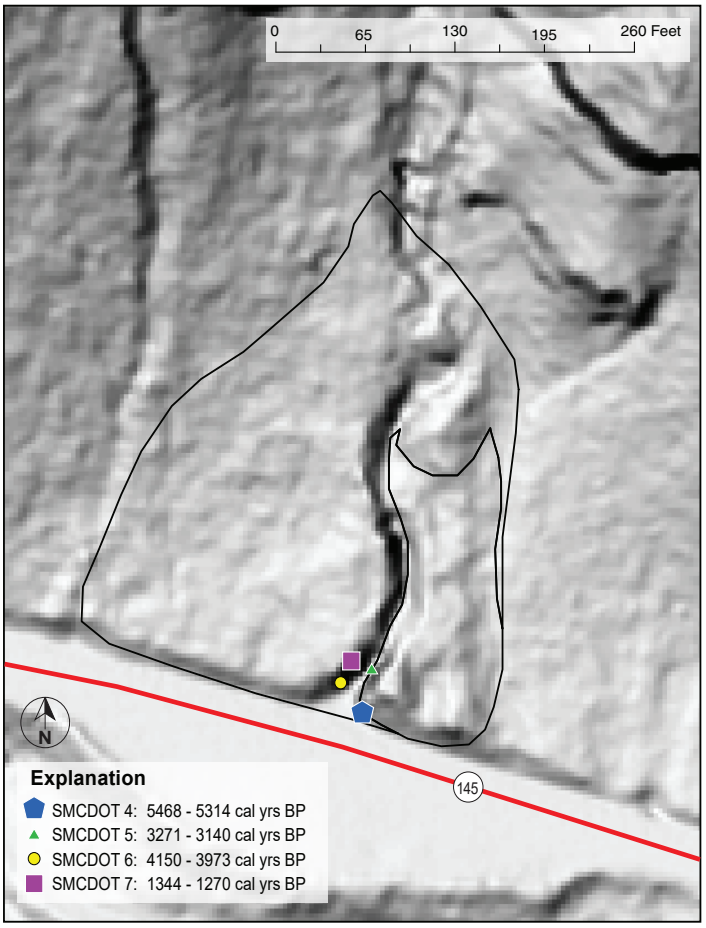

Figure 12. Distribution of ^{14}C age estimates at Fan B. The distribution of ages across the sampled area may indicate a lateral fan migration at this site.

6. DISCUSSION

6.1 Carbon-14 and Optically Stimulated Luminescence

Debris-flow deposits were thought to be unlikely candidates for OSL analysis because quartz grains are more likely to be partially bleached due to chaotic flow, high sediment entrainment ratios, short transport distances, and rapid deposition. However, single-grain analysis can help constrain ages of debris flows, even when full resetting of quartz luminescence is not achieved. While high overdispersion is still likely and present in many cases, applying specific age models to OSL data can help constrain and yield accurate age estimates (Steve Forman, written commun., 2020). Several studies have applied SAR methods and the MAM to debris-flow deposits in order to obtain reliable age estimates from samples that return higher dose distributions (Schmidt and others, 2012; Hoyos and others, 2015; Lang, 2013; Zhao and others, 2017).

Efforts have been made to compare the reliability of data yielded by ^{14}C to OSL. Kim and others (2013) dated ancient soils in Korea. The dated unit underwent complete bleaching which may differ from the process by which debris-flow sediments are deposited as described above. However, in this study, Kim and others (2013) found that the OSL samples yielded more reliable ages for reconstructing the site's absolute chronology. Lee and others (2011) compared ^{14}C and OSL samples taken from lake sediments in Mongolia. In this study they found the OSL to be more reliable than the ^{14}C. Old carbon was contributed to the system by eolian sediments derived from older soils and units in the region yielding older ^{14}C ages estimates than OSL estimates.

6.2 Carbon-14 and Sample SMCDOT 8

Bulk ^{14}C analysis can yield a general estimation of the age of the soil sampled but has proven to provide over or underestimations due to the influx of carbon to soil profiles. While the majority of the ^{14}C samples, except for SMCDOT 8 (discussed below) are self-consistent, they do not correlate well with the three OSL results.

The lab identified an apparent charcoal fragment submitted with the bulk ^{14}C sample collected at SMCDOT 8. The "charcoal" fragment yielded an age beyond the lower limit (>43,500 cal yrs BP) for carbon analysis. Sample SMCDOT 8 was collected stratigraphically higher than SMCDOT 1, which produced an age estimate of 28,011 – 27,660 cal yrs BP. Therefore, reliability of SMCDOT 8 is low given its stratigraphic relationship with SMCDOT 1. The coal fragment analyzed may be sourced from local bedrock units which could account for the apparent discrepancy in ages between the samples. Additional sample material for SMCDOT 8 was submitted for ^{14}C analysis but could not be analyzed due to low carbon content. Therefore, the age returned for SMCDOT 8 was not used in this study.

6.3 Fan A

Age estimates calculated from carbon samples collected at Fan A yielded a range between 28,011 and 8,971 cal yrs BP. Assuming the carbon samples are accurate, samples SMCDOT 3 (12,819 – 12,707 cal yrs BP), SMCDOT 9 (16,905 – 16,432 cal yrs BP), and SMCDOT 10 (9,037 – 8,971 cal yrs BP) may correlate with the end of the Pinedale Glaciation (21,000 to 12,300 years BP) and wetter climate conditions. Samples SMCDOT 1 (28,011 – 27,660 cal years BP) and SMCDOT 2 (25,051 – 24,425 cal years BP) are older than the glacial maximum (~23,500 – 21,000 years BP) during the Pinedale Glaciation (Clark and others, 2009).

Assuming the carbon samples are not accurate, an influx of older carbon potentially derived from forest fires could have infiltrated the soils developed on the debris-flow deposits at Fan A. Samples collected from Fan A, except for SMCDOT 1, were collected less than 90 cm below ground surface. The influx of old carbon may contaminate the ^{14}C samples resulting in an older age estimate than the OSL sample at SMCDOT 3.

The OSL analysis of sample SMCDOT 3 yielded an age estimate of 1,985 ± 210 yrs BP, which is considerably younger than any other age estimates reported in this study and not associated with any known periods of glaciation. However, the regional climate has cycled between periods of higher precipitation and aridity throughout the Holocene (Carrara, 2011). Carbon dating of charcoal from debris-flow deposits in the nearby Animas Valley indicates that before 2,000 cal yrs BP and after 1,400 cal yrs BP, the region's climate may have been more arid (Bigio and others, 2017). Assuming the age estimate is accurate, the date yielded by SMCDOT 3 correlates with the beginning of a period during the Late Holocene that may have experienced higher precipitation levels. The higher overdispersion associated with the sample could be accounted for by an influx of younger sediment to the sample location, since it was collected within 1 m of the ground surface. This could contribute to potential inaccuracy of the age estimate yielded by the sample.

6.4 Fan B

Age estimates calculated from ^{14}C samples collected at Fan B yielded a range between 5,468 and 1,270 cal yrs BP. Assuming the carbon samples are accurate, sample SMCDOT 7 (1,344 – 1,270 cal yrs BP) falls within a period of high fire

severity from 1,400 – 1,175 cal yrs BP (Bigio and others, 2017) when the climate may have been dryer. The other three ^{14}C samples are older than the fire severity cycles documented by Bigio and others (2017). Sample SMCDOT 5 (3,271 – 3,140 cal yrs BP) correlates with a wetter climate period between 3,300 and 2,700 cal yrs BP (Asmerom and others, 2007). Sample SMCDOT 4 (5,468 – 5,314 cal yrs BP) may also correlate with a wetter climate period documented by Asmerom and others (2007). However, SMCDOT 6 (4,150 – 3,973 cal yrs BP) correlates with a drier climate documented by Asmerom and others (2007).

Sample SMCDOT 6 is stratigraphically lower (0.9 m) than SMCDOT 4, but the ^{14}C sample at SMCDOT 6 yielded a younger age estimate (4,150 – 3,973 cal yrs BP) than SMCDOT 4 (5,468 – 5,314 cal yrs BP). Assuming the ages estimated by ^{14}C samples are reliable, accommodation space adjacent to the fan sampled by SMCDOT 4 could account for the younger age estimate yielded from SMCDOT 6. In other words, the debris-flow deposit sampled by SMCDOT 4 occurred approximately 5,468 – 5,314 cal yrs BP, leaving the sample location higher in the landscape than the accommodation space adjacent to it. The debris-flow represented by SMCDOT 6 occurred approximately 4,150 – 3,973 cal yrs BP, filling the available accommodation space adjacent to the older fan.

The OSL age estimates contradict this relationship. Sample SMCDOT 4 (OSL) returned an age estimate younger than SMCDOT 6 (OSL) which would indicate a younging-upwards progression of deposition starting from oldest deposits at the bottom and younger deposits higher in the section. Discrepancies between the bulk carbon and OSL age estimates are more difficult to reconcile at Fan B. The atmosphere or vegetation may have contributed younger carbon to the sampled soil profile to produce younger age estimates.

A glacier likely covered the area underlying Fan B during the Pinedale Glaciation (Figure 5) (Carrara, 2011). Deglaciation of the region started around 21,000 to 19,400 years BP and culminated by approximately 14,000 to 12,300 years BP (Leonard and others, 2017; Ward and others, 2009; Schweinsberg and others, 2020; Guido and others, 2007). Samples SMCDOT 4 and 6 yielded statistically reliable ages by OSL analysis; 12,312 ± 530 and 14,910 ± 720 yrs BP, respectively. These ages correlate well with the end of the Pinedale Glaciation in the region and indicate that ice would have receded by at least 15,000 yrs BP at this site.

7. CONCLUSIONS

Strong correlations between known periods of wetter climate during the Late Pleistocene and Holocene cannot be made for every ^{14}C sample. However, several samples are correlative with wetter periods associated with the end of the Pinedale Glaciation and identified in fire-severity and speleothem growth records (Bigio and others, 2017; Asmerom and others, 2007). No charcoal or other organic material was present in any of the carbon samples collected, except for SMCDOT 8 which yielded an age beyond the lower limit. Bulk carbon samples may yield inaccurate age estimates as compared to charcoal or organic material, especially when samples are collected within the uppermost 1.5 m.

While three OSL samples is not enough to identify a strong correlation between age estimates and climate conditions that could contribute to debris-flow initiation, the samples do correlate with documented periods of wetter climate in the region. Additionally, the samples yielded age estimates with lower over-dispersion ratios. This indicates OSL sampling may be a viable method to estimate the ages of debris-flow deposits.

Two samples, SMCDOT 3 (OSL) and SCDMOT 7 (^{14}C), yielded age estimates that could help establish a debris-flow recurrence interval during the Late Holocene. Generally, debris flow initiation in modern times is associated with periods of above average precipitation, post-wildfire conditions, rapid snowmelt, or some combination there of. Erosion-initiated debris flow can occur in arid to semiarid environments in areas with minimal vegetation and loose soil during normal rainfall events. Additional samples are needed in order to establish a reliable recurrence interval and make correlations between climate and debris-flow initiation in the region during the Late Holocene. None of the samples yielded age estimates that can contribute to a modern recurrence interval.

8. FUTURE WORK

The data collected as a part of this pilot study provides a framework for future debris-flow dating in San Miguel County. We have several recommendations for future work:

1. Dating younger deposits that may exist higher in the landscape above the sampling locations at both sites. Dating these younger deposits can help constrain the modern (<50 yrs) recurrence interval.
2. Increased sampling density, both vertically and laterally. Increased vertical sampling can help constrain the recurrence interval and estimate magnitude while increase lateral sampling can help identify historical avulsion patterns.
3. Use OSL analysis for future samples to determine if the method is consistently accurate for estimating the ages of debris-flow deposits.

Lastly, rain gauge and soil moisture sensors could be deployed near debris-flow initiation sites to measure precise precipitation levels. Correlating debris-flow events with historical precipitation records may also be useful for infrastructure management and debris-flow prediction. Accurate event magnitude estimation and depositional pattern identification, in conjunction with proper instrumentation, is essential when evaluating debris-flow susceptibility. Emergency management teams could use a more precise forecasting system to deploy hazard mitigation protocols and design appropriate mitigation structures that increase roadway safety.

9. REFERENCES

Arnold, L.J., and Roberts, R.G., 2009, Stochastic modelling of multi-grain equivalent dose (De) distributions – Implications for OSL dating of sediment mixtures: Quaternary Geochronology, v. 4, no. 3, p. 204–230.

Asmerom, Y., Polyak, B., Burns, S., and Rassmussen, J., 2007, Solar forcing of Holocene climate change – New insights from a speleothem record, southwestern United States: Geology, v. 35, no. 1, 4 p.

Atwood, W.W., and Mather, K.F., 1932, Physiography and Quaternary geology of the San Juan Mountains, Colorado: U.S. Geological Survey Professional Paper 166, 176 p.

Benson, L., Madole, R., Landis, G., and Gosse, J., 2005, New data for Late Pleistocene Pinedale alpine glaciation from southwestern Colorado: Quaternary Science Reviews, v. 24, no. 1-2, p. 49–65.

Bigio, E., Thomas, W.S., and Pearthtree, P.A., Late Holocene fire-climate relationships of the western San Juan Mountains, Colorado: International Journal of Wildland Fire, v. 26, p. 944–962.

Bush, A.L., Bromfield, C.S., and Pierson, C.T., 1959, Areal geology of the Placerville quadrangle, San Miguel County, Colorado: Geological Survey Bulletin 1072-E, scale 1:24,000.

Bush, A.L., Bromfield, A.S., Marsh, O.T., and Taylor, R.B., 1961, Preliminary geologic map of the Gray Head quadrangle, San Miguel County, Colorado: U.S. Geological Survey, Mineral Investigations Field Studies Map MF-176, scale 1:24,000.

Carrara, P.E., 2011, Deglaciation and postglacial treeline fluctuation in the Northern San Juan Mountains, Colorado: U.S. Geological Survey Professional Paper 1782, 48 p.

Clark, P.U., Dyke, A.S., Shakun, J.D., Carlson, A.E., Clark, J., Wohlfarth, B., Mitrovica, J.X., Hostetler, S.W., and McCabe, A.M., The last glacial maximum: Science, v. 325, p. 710–714.

Crovelli, R.A., 2000, Probability models for estimation of number and costs of landslides: U.S. Geological Survey, OF-00-249, 23 p.

Durcan, J.A., and Duller, G.A.T., 2011, The fast ratio – A rapid measure for testing the dominance of the fast component in the initial OSL signal from quartz: Radiation Measurements, v. 46, no. 10, p. 1065–1072.

Fain, J., Soumana, S., Montret, M., Miallier, D., Pilleyre, T., and Sanzelle, S., 1999, Luminescence and ESR dating-Beta-dose attenuation for various grain shapes calculated by a Monte-Carlo method: Quaternary Science Reviews, v. 18, no. 2, p. 231–234.

Forman, S.L., Tripaldi, A., and Ciccioli, P.L., 2014, Eolian sand sheet deposition in the San Luis paleodune field, western Argentina as an indicator of a semi-arid environment through the Holocene: Paleogeography, Paleoclimatology, Paleoecology v. 411, p. 122–135.

Forman, S.L., 2015, Luminescence Dating in Paleoseismology, *in* Beer, M., Kougioumtzoglou, I. A., Patelli, E., and Au, SK., eds., Encyclopedia of Earthquake Engineering: Springer Berlin Heidelberg, p. 1371–1378.

Galbraith, R.F., Roberts, R.G., Laslett, G.M., Yoshida, H., and Olley, J.M., 1999, Optical dating of single and multiple grains of quartz from Jinmium rock shelter, northern Australia, part 1, Experimental design and statistical models: Archaeometry, v. 41, no. 2, p. 339–364.

Galbraith, R.F., and Roberts, R.G., 2012, Statistical aspects of equivalent dose and error calculation and display in OSL dating – An overview and some recommendations: Quaternary Geochronology, v. 11, p. 1–27.

Guerin, G., Mercier, N., and Adamiec, G., 2011, Dose-rate conversion factors – Update: Ancient TL, v. 29, no. 1, p. 5–8.

Guido, Z.S., Ward, D.J., and Anderson, R.S., 2007, Pacing the post – Last glacial maximum demise of the Animas Valley Glacier and the San Juan Mountain ice cap, Colorado: Geology, v. 35, no. 8, p. 739–742.

Guo, X., Forman, S.L., Marin, L., and Li, X., 2018, Assessing tectonic and climatic controls for Late Quaternary fluvial terraces in Guide, Jianzha, and Xunhua basins for the Yellow River on the northeastern Tibetan Plateau: Quaternary Science Reviews., v. 195, p. 109–121.

Hoyos, N., Monsalve, O., Berger, G.W., Antinao, J.L., Giraldo, H., Silva, C., Ojeda, G., Bayona, G., Escobar, J., and Montes, C., 2015, A climatic trigger for catastrophic Pleistocene-Holocene debris flows in the Eastern Andean Cordillera of Colombia: Journal of Quaternary Science, v. 30., no. 3, p. 258–270:

Kim, M.J., Jung, B.G., Kim, S.Y., and Hong, D.G., 2013, Comparison of OSL and ^{14}C dates estimeated from Paleolithic paleosol of the Suheol-Ri Fan in Cheonan, Korea: Mediterranean Archaeology and Archaeometry, v. 13, no. 3, p. 117–126.

Lang, A., 2013, Luminescence dating of alluvial fans and cones, *in* Schneuwly-Bollschweiler, M., Stoffel, M., and Rudolf-Miklau, F., eds., Dating torrential processes on fans and cones—Methods and their application for hazard and risk assessment: Advances in Global Research, v. 47, p. 283–295.

Lee, M.K., Lee, Y.I., Lim, H.S., Lee, J.I., Choi, J.H., Yoon, H.I., 2011, Comparison of radiocarbon and OSL dating methods for a Late Quaternary sediment core from Lake Ulaan, Mongolia: Journal of Paleolimnology, v. 45, p. 127–135.

Leonard, E.M., Laabs, B.J.B., Schweinsberg, A.D., Russell, C.M., Briner, J.P., and Young, N.E., 2017, Deglaciation of the Colorado Rocky Mountains following the Last Glacial Maximum: Cuadernos de Investigación Geográfica, v. 43, no. 2, p. 497–526.

Mejdahl, V., and Christiansen, H.H., 1994, Procedures used for luminescence dating of sediments: Quaternary Science Review, v. 13, no. 5-7, p. 403–406.

Murray, A.S., and Wintle, A.G., 2003, The single aliquot regenerative dose protocol – Potential for improvements in reliability: Radiation Measurements, v. 37, no. 4-5, p. 377–381.

Onken, J., and Forman, S.L., 2017, Terminal Pleistocene volcanic eruptions at Zuni Salt Lake, west-central New Mexico, USA: Bulletin of Volcanology, v. 79, no. 10, 17 p.

Peng, L., and Forman, S.L., 2019, LDAC – An Excel-based program for luminescence equivalent dose and burial age calculations: Ancient TL, v. 37, no. 2, p. 21–40.

Pierson, T.C., 2005, Distinguishing between debris flow and floods from field evidence in small watersheds: U.S. Geologic Survey, Fact Sheet 2004-3142, 4 p.

Prescott, J.R., and Hutton, J.T., 1994, Cosmic ray contributions to dose rates for luminescence and ESR dating: large depths and long-term time variations: Radiation Measurements, v. 23, no. 2-3, p. 497–500.

Quantum Spatial, 2018, CWCB NASA re-process, Colorado priority sites lidar: Quantum Spatial, Corvallis, OR, 30 p.

Schmidt, S., Tsukamoto, S., Salomon, E., Frechen, M., and Hetzel, R., 2012, Optical dating of alluvial deposits at the orogenic front of the Andean Precordillera, Mendoza, Argentina: Geochronometria, v. 39, no. 1, p. 62–75.

Schweinsberg, A.D., Briner, J.P., Licciardi, J.M., Shroba, R.R., and Leonard, E.M., 2020, Cosmogenic 10 Be exposure dating of Bull Lake and Pinedale moraine sequences in the upper Arkansas River valley, Colorado Rocky Mountains, USA: Quaternary Research, v. 97, p. 125–139.

Ward, D.J., Anderson, R.S., Guido, Z.S., and Briner, J.P., 2009, Numerical moderling of cosmogenic deglaciation records, Front Range and San Juan mountains, Colorado: Journal of Geophysical Research, v. 114, no. F1, 21 p.

Wintle, A.G., and Murray, A.S., 2006, A review of quartz optically stimulated luminescence characteristics and their relevance in single-aliquot regeneration dating protocols: Radiation Measurements, v. 41, no. 4, p. 369–391.

Wright, D., Forman, S.L., Waters, M., and Ravesloot, J., 2011, Holocene eolian activity as a proxy for broad-scale landscape change on the Gila River Indian Community, Arizona: Quaternary Research, v. 76, no. 1, p. 10–21.

Zhao, Q., Thomsen, K.J., Murray, A.S., Wei, M., and Song, B., 2017, Single-grain quartz OSL dating of debris flow deposits from Men Tou Gou, southwest Beijing, China: Quaternary Geochronology, v. 41, p. 62–69.

APPENDIX A

Optically Stimulated Luminescence Dating Methods

Optically stimulated luminescence (OSL) is a technique that dates the burial time of quartz grains. The time-zeroing mechanism is the exposure of grains to >1 min of sunlight. There is subsequent time-signal acquisition with burial, shielding from sunlight, and exposure to ionizing radiation, mostly from radioactive decay during the burial period (Forman, 2015). Optically stimulated luminescence dating methods have been used previously in numerous geomorphic settings to provide chronologic control in the absence of organic material for radiocarbon dating (e.g., Forman, 2015; Guo and others, 2018; Onken and Forman, 2017). Each aliquot contained approximately 20 to 100 quartz grains corresponding to a 1-millimeter or less circular diameter of grains adhered (with silicon) to a 1 cm-diameter, circular, aluminum disc. The quartz fraction was sieved and isolated by density separation using the heavy liquid Na–polytungstate (2.4 and 2.6 g/cc) for a specific grain-size range (e.g., 250-100 μm), then exposed to at least one 40-minute immersion in hydrofluorosilicic acid (HF 40%) to etch the outer portion of the grains (~10 μm) affected by alpha radiation (Mejdahl and Christiansen, 1994). The isolated quartz fraction was rinsed finally in HCl (10%) to remove any insoluble fluorides (cf. Forman and others, 2014).

The optical purity of quartz separates was tested by exposing aliquots to infrared excitation (1.08 watts from a laser diode at 845 ± 4 nm), which often preferentially excites feldspar minerals. Laboratory staff repeated the HF 40-minute immersion if this test indicated feldspar contamination. Another safeguard for determining quartz grain purity was examining a small subsample with a visualized petrographic microscope and Raman spectroscopy. If a subsample exhibited > 1% non-quartz minerals, particularly feldspar minerals, laboratory staff re-treated them with density separations, HF soaking for an additional 20 or 40 minutes, sieved again and rechecked for grain purity.

The single-aliquot regenerative-dose (SAR) analyses used an Automated Risø TL/OSL–DA–15 system. Blue light excitation (470 ± 20 nm) was from an array of 30 light-emitting diodes that deliver ~15 mW/cm^2 to the sample position at 90% power. Optical stimulation for all samples was completed at an elevated temperature (125° C) using a heating rate of 5 °C/s. All SAR emissions were integrated for the first 0.8 s of stimulation out of 40 s of measurement, with background emissions integrated for the last ten seconds of data collection for the 30 to 40 s interval. The luminescence emission for all quartz fractions showed a dominance of a fast component, with > 90% diminution of luminescence after 4 seconds of excitation with blue light. Laboratory scientists calculated the fast ratio for both natural and equivalent emissions for each aliquot's regenerative dose (Durcan and Duller 2011). Aliquots were removed from the final equivalent dose analysis if they had a fast ratio of <15 and an infrared depletion ratio of > 5%.

Before applying SAR dating protocols, laboratory staff performed a series of experiments to evaluate the effect of preheating at 160, 180, 200, 220, and 240 °C on isolating the most robust time-sensitive and thermal transfer emissions of the regenerative signal. These experiments entailed giving a known dose (10 Gy) and evaluating which preheat resulted in the recovery of this dose. There was concordance with the known dose (40 Gy) for preheat temperatures above 180 °C with an initial preheat temperature of 200 °C for 10 s in the SAR protocols. Staff applied a second "cut heat" at 180 °C for 10 s before the measurement test dose measurement and then a final heating at 260 °C for 40 s to minimize carryover of luminescence to the succession of regenerative doses. A test for the reproducibility of the radiation-induced SAR ratio (L_x/T_x) was also performed by giving the same beta ($^{90}Sr/^{90}Yt$) source radiation exposure for the initial and the final regenerative dose and evaluating the concordance of the SAR ratios, which should be within 10% (Murray and Wintle, 2003; Wintle and Murray, 2006).

Aliquots used for equivalent dose calculations were required to have a fast ratio < 15 (Durcan and Duller, 2011), a recycling ratio between 0.9 to 1.10, a zero-dose test of > 5% of the natural signal, and errors in equivalent dose of <10%. (Murray and Wintle, 2003; Wintle and Murray, 2006). Modeling of the regenerative growth curves uses the exponential plus linear or quadratic form. Error analysis for equivalent dose calculations for individual quartz aliquots assumed a measurement error of 1% with 2000 Monte Carlo simulation repeats to characterize errors better.

An overdispersion percentage of a D_e distribution estimates the relative standard deviation from a central D_e value in the context of a statistical estimate of errors (Galbraith and others, 1999; Galbraith and Roberts, 2012). A zero overdispersion percentage indicates high internal consistency in D_e values when 95% of the D_e values are within 2σ errors. Overdispersion values < 25% are routinely assessed for quartz grains with well solar resetting, like eolian sands (e.g., Wright and others, 2011; Forman and others, 2014). The central age model developed by Galbraith and others (1999) is applied when overdispersion values are < 25%. Overdispersion values > 25% indicate mixing of grains of various ages or partial solar resetting of grains; the minimum age model (MAM;

four parameters) may be an appropriate statistical treatment for such data. The MAM can effectively model the D_e components that are time-dependent and inherited (Galbraith and Roberts, 2012; Peng and Forman, 2019). However, some studies have concluded that overdispersion values between 20 and 32% may reflect a single De population, especially if the D_e distribution is symmetrical. In this case, the dispersion could be related to variability associated with micro-dosimetry, sedimentary processes, or both (e.g., Arnold & Roberts, 2009). We consider overdispersion values > 20% indicative of non-age-related processes such as post-depositional mixing of grains of various ages, partial solar resetting of grains, or complex microdosimetry.

The environmental dose rate (D_r) is a critical measurement for calculating a luminescence age. The D_r is an estimate of quartz grains' exposure to ionizing radiation from the decay of the U and Th series, ^{40}K, Rb, and cosmic sources during the burial period. The U, Th, Rb, and K concentrations are determined on the bulk sediment by inductively coupled plasma mass spectrometry by ALS Laboratories, Reno, Nevada. The beta and gamma doses are adjusted according to grain diameter to compensate for mass attenuation for the dose rate (Fain and others, 1999; Guerin and others, 2011). A cosmic ray component is calculated using location, elevation, and depth of strata sampled. Results are between 0.17 and 0.30 mGy/yr and include the soft component (Prescott and Hutton, 1994; Peng and Forman, 2019).

There is uncertainty in assessing the moisture content of a sample during the burial period. We estimated moisture content (by weight) from present values, particle size characteristics and by using field indicators to identify the height of the water table or possible perched water tables. Systematic and random errors for final ages are calculated in a quadrature at one standard deviation by the Luminescence Dating and Age Calculator (LDAC) at https://www.baylor.edu/geosciences/index.php?id=962356 (Peng and Forman, 2019). The datum year for all OSL ages is AD 2010.

APPENDIX B

Figure B1 Profile description

Unit 1: 0-0.3 m. Colluvium. The unit is poorly sorted sand to coarse pebble and cobble gravel. There are no carbonate rinds and no visible carbonate nodules in the matrix, but it does effervesce when treated with 10% dilute hydrochloric acid (HCl). There is no other visible soil development.

Unit 2: 0.3-0.75 m. Debris flow. The unit is matrix-supported and has a weak coarsening upward depositional sequence. The matrix is clay to coarse, quartz-rich sand. Sand grains are angular. Clasts are mostly angular to subangular sandstone and as much as 25 cm in diameter. Clasts are chiefly light-gray to tan, non-calcareous, quartz-rich sandstone. There are no carbonate rinds on the clasts and no visible carbonate nodules in the matrix. However, the matrix does effervesce when treated with HCl. Bulk carbon and OSL sample SMCDOT 8 were taken approximately 0.5 m bgs (below ground surface) in a pocket of fine to medium sand.

Unit 3: 0.75-1.5 m. Debris flow. The unit is matrix-supported and has a weak coarsening upward depositional sequence. The matrix is clay to medium, quartz-rich sand. Sand grains are angular. Clasts are mostly angular to subangular sandstone and as much as 70 cm in diameter. Clasts are mostly light gray to tan, non-calcareous, quartz-rich sandstone. There are no carbonate rind on the clasts and no visible carbonate nodules in the matrix, but it effervesces when treated with HCl. Bulk carbon and OSL samples SMCDOT 1 were taken approximately 1.5 m bgs in a pocket of fine to medium sand.

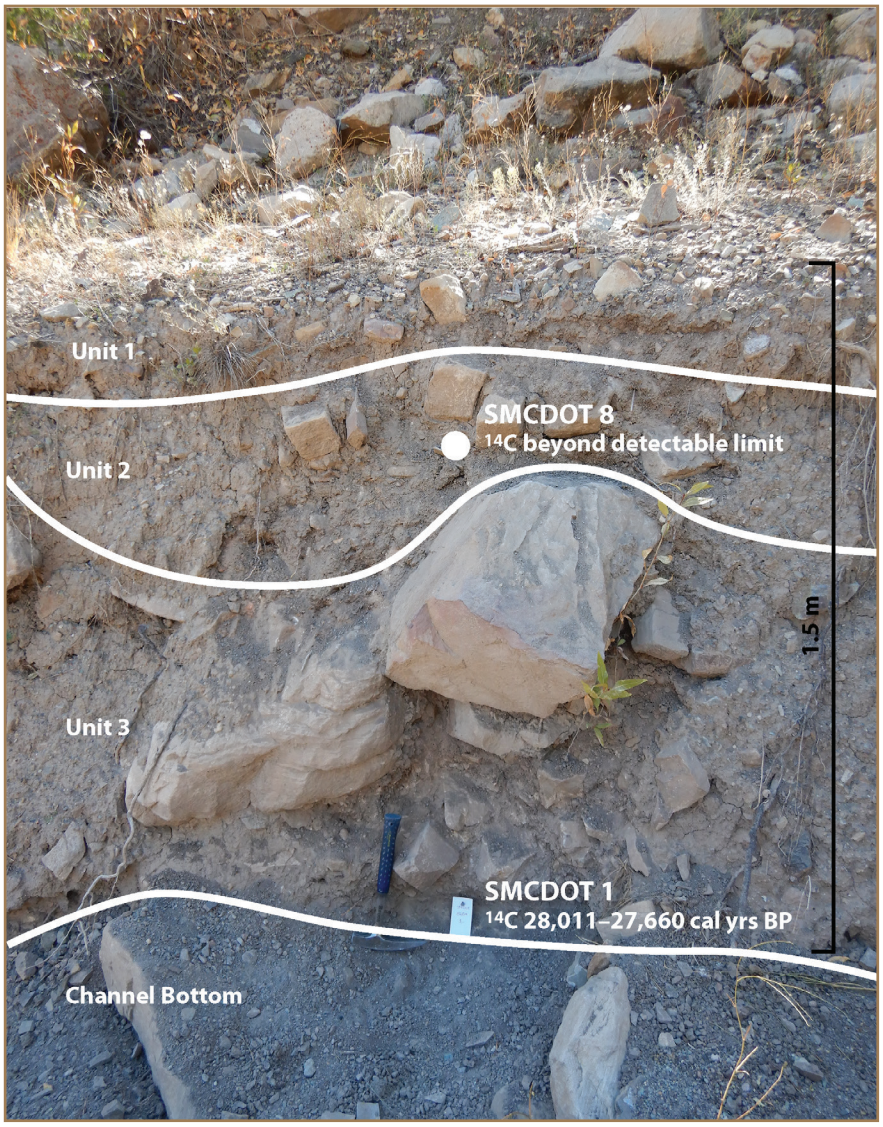

Figure B1. Fan A, SMCDOT 1 and 8. White lines represent approximate contacts between units. Sample SMCDOT 1 was taken approximately 1.5 m below ground surface (paper marker right of hammer). Bulk carbon analysis yielded an age estimate of 28,011-27,660 cal yrs BP. Sample SMCDOT 8 was taken approximately 0.4 m below ground surface. Carbon analysis returned an age estimate beyond lower limit (>43,500 cal yrs BP).

Figure B2 Profile description

Unit 1: 0-0.4 m. Debris flow. The unit is matrix supported. The matrix is clay to fine, quartz-rich sand and effervesces moderately when treated with HCl even though there are no visible secondary carbonate nodules. Clasts are angular to subangular and as much as 25 cm in diameter. Thin (< 1 mm), moderately continuous carbonate rinds exist on the base of clasts. Bulk carbon and OSL sample SMCDOT 9 were taken 15 cm bgs in medium sand.

Unit 2: 0.4-1 m. Debris flow. The unit is matrix supported. The matrix is clay to medium, quartz-rich sand. Clasts are angular to subangular and as much as 30 cm in diameter. Thin (< 1 mm), moderately continuous carbonate rinds exist on the base of clasts. Bulk carbon and OSL samples SMCDOT 2 were taken 76 cm bgs in medium sand to fine pebbles.

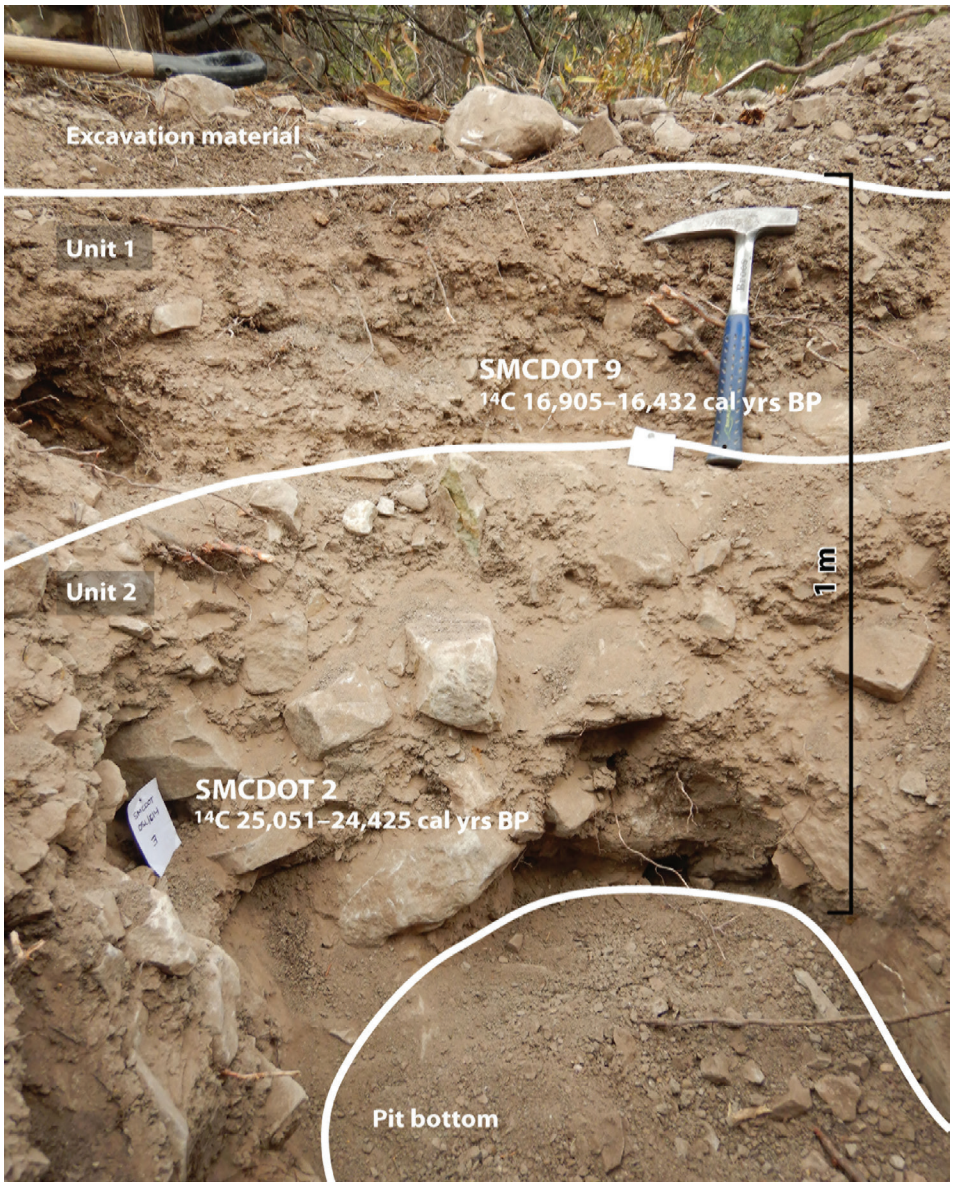

Figure B2. Fan A, SMCDOT 2 and 9. White lines represent approximate contacts between units. Sample SMCDOT 2 was taken approximately 0.76 m below ground surface (paper marker left of hammer). Bulk carbon analysis yielded an age estimate of 25,051-24,425 cal yrs BP. Sample SMCDOT 9 was taken approximately 15 cm below ground surface (paper marker left of hammer). Bulk carbon analysis yielded an age estimate of 16,905-16,432 cal yrs BP.

Figure B3 Profile description

Unit 1: 0-0.4 m. Debris flow. The unit is matrix supported. The matrix is clay to coarse, quartz-rich, angular sand. The matrix effervesces readily when treated with HCl, however, there are no secondary carbonate nodules present in the soil. Clasts are angular to subangular, and as much as 15 cm in diameter. Clasts are more prevalent in Unit 1 than Unit 2. Some clasts have thin (<1 mm), discontinuous carbonate rinds on their bases. Bulk carbon and OSL samples SMC-DOT 10 taken were 40 cm bgs in a pebbly sand pocket between gravel clasts.

Unit 2: 0.4-0.9 m. Debris flow or hyperconcentrated flow. The unit is matrix supported. The matrix is clay to medium, quartz-rich, angular sand, and effervesces readily when treated with HCl. However, no secondary carbonate is present in the soil. Clasts are angular to subangular and as much as 15 cm in diameter. Bulk carbon and OSL samples SMC-DOT 3 were taken 70 cm bgs in sandy material.

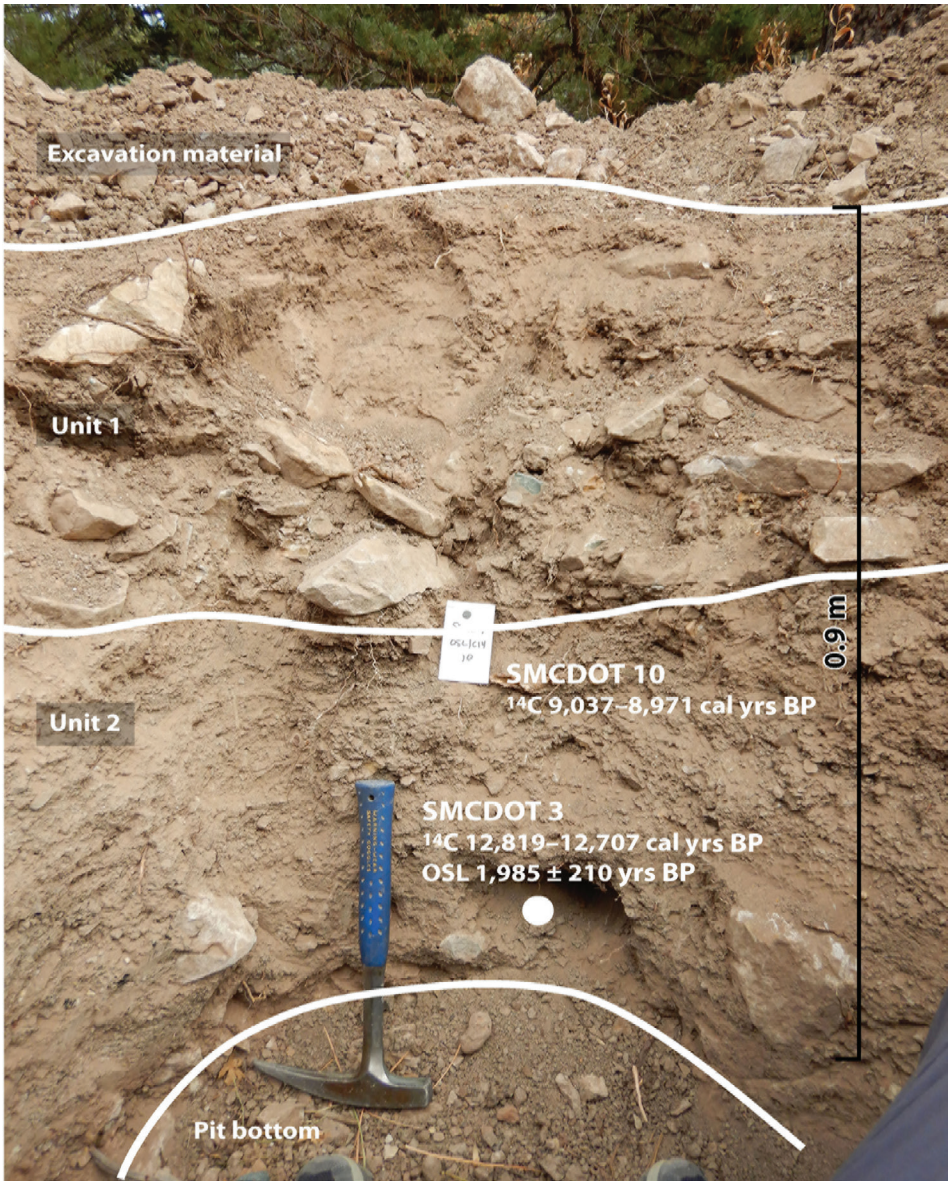

Figure B3. Fan A, SMCDOT 3 and 10. White lines represent approximate contacts between units. Sample SMCDOT 3 was taken approximately 70 cm below ground surface (white dot right of hammer). Bulk carbon analysis yielded an age estimate of 12,819-12,707 cal yrs BP. Optically stimulated luminescence analysis yielded an age estimate of 1,985 ± 210 yrs BP. Sample SMCDOT 10 was taken approximately 40 cm below ground surface (paper marker above hammer). Bulk carbon analysis yielded an age estimate of 9,037 – 8,971 cal yrs BP.

Figure B4 Profile description

Unit 1: 0-0.9 m. Colluvium or debris flow. Gravel clasts are angular to subangular and as much as 50 cm in diameter. The unit was not accessible from the channel.

Unit 2: 0.9-3 m Debris flow. The unit is matrix supported and has a coarsening upward depositional sequence. Clasts are angular to subangular and as much as 1.2 m in diameter. The unit was not accessible from the channel.

Unit 3: 3-4.75 m. Debris flow. The unit is matrix supported and has a coarsening upward depositional sequence. The matrix is clay to fine, quartz-rich, angular sand. A minor fraction of the matrix is coarse sand to fine pebbles. Clasts are angular to subangular and as much as 1.5 m in diameter. There is no visible soil development and no visible secondary carbonate development in the matrix. However, the matrix effervesces when treated with HCl. Bulk carbon and OSL samples SMCDOT 4 were taken approximately 4.6 m bgs in sandy material.

Unit 4: 4.75-5.8 m. Potentially a debris flow but most of the unit is obscured by colluvium.

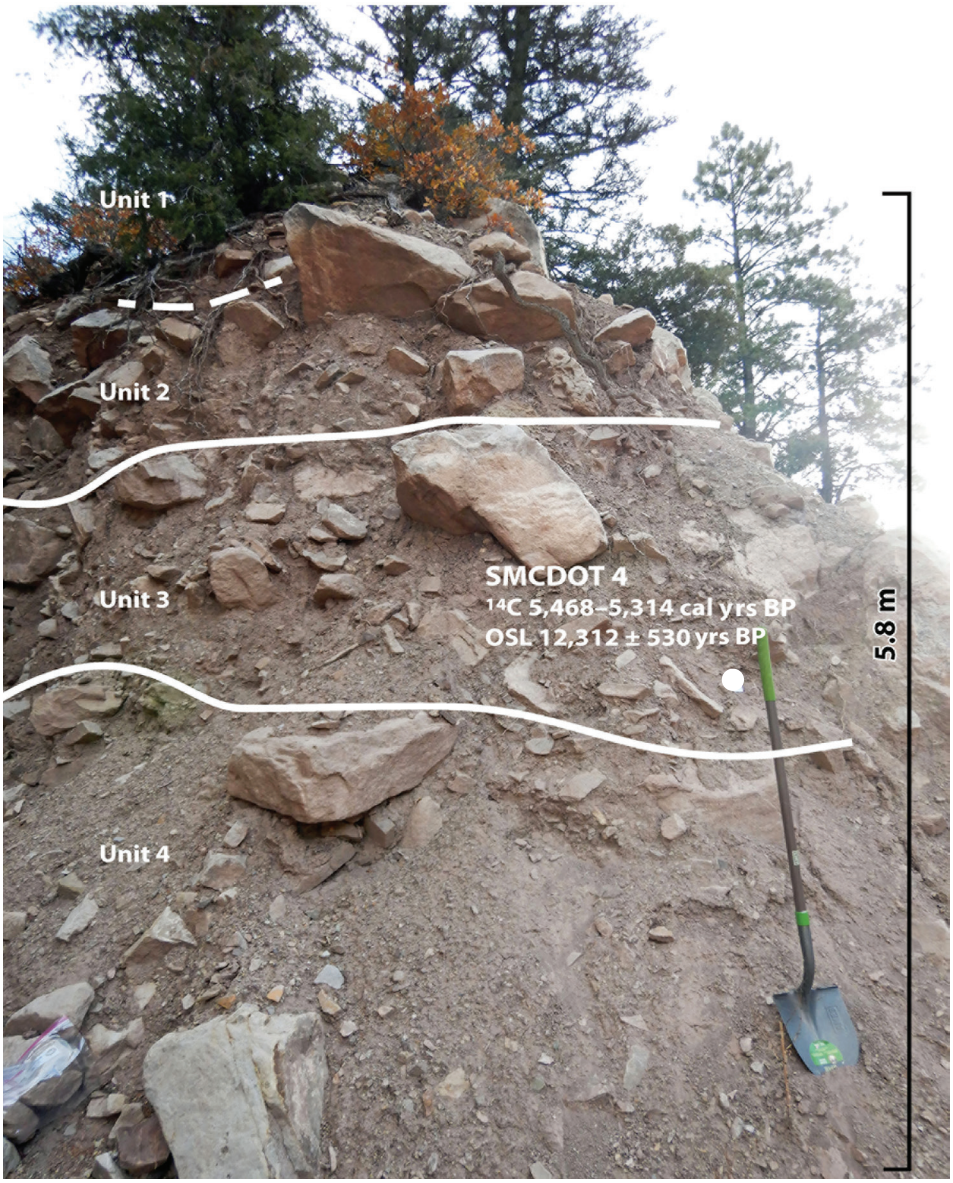

Figure B4. Fan B, SMCDOT 4. White lines represent approximate contacts between units. Sample SMCDOT 4 was taken approximately 4.6 m below ground surface (white dot left of shovel handle). Bulk carbon analysis yielded an age estimate of 5,468-5,314 cal yrs BP. Optically stimulated luminescence analysis yielded an age estimate of 12,312 ± 530 yrs BP.

Figure B5 Profile description

Unit 1: 0-0.9 m. Colluvium or debris flow. The unit is correlative with Unit 1 from Figure A4. Clasts are angular to subangular and as much as 50 cm in diameter. The unit was not accessible from the channel.

Unit 2: 0.9-3.5 m. Debris flow. The unit is correlative with Unit 2 from Figure A4. It is matrix supported and has a coarsening upward depositional sequence. The matrix is clay to medium, quartz-rich, angular sand. Clasts are angular to subangular throughout the unit and range from 10 cm in diameter at the base of the unit to 1.5 m in the upper portion of the unit. There is no visible secondary carbonate development in the matrix and no carbonate rinds on the clasts. However, the matrix effervesces slightly when treated with HCl. There is no visible soil development. Bulk carbon and OSL samples SMCDOT 5 were taken 3.5 m bgs in sandy material.

Unit 3: Below 3.5 m. Debris flow. The unit is correlative with Unit 3 from Figure A4. It is matrix supported and has a coarsening upward depositional sequence. The matrix is clay to coarse, quartz-rich, angular sand. Clasts angular to subangular and as much as 1.5 m in diameter. Secondary carbonate development is not visible in the matrix. However, the matrix effervesces when treated with HCl. Carbonate rinds on clasts are overturned. There is no visible soil development.

Figure B5. Fan B, SMCDOT 5. White lines represent approximate contacts between units. A sample was collected from the upper hole but was unsatisfactory; therefore, the location was resampled from the lower hole (white dot). Sample SMCDOT 5 was taken approximately 3.5 m below ground surface. Bulk carbon analysis yielded an age estimate of 3,271-3,140 cal yrs BP.

Figure B6 Profile description

Unit 1: 0-0.9 m. Debris flow or colluvium. Clasts are as much as 2.5 m in diameter. The unit was not accessible from the channel.

Unit 2: 0.9-2.1 m. Debris flow. The unit is matrix supported. The matrix is clay to medium, quartz-rich, subangular to subround sand, and effervesces when treated with HCl. However, there is no visible secondary carbonate in the matrix. Clasts are angular to subangular, sandstone, mudstone, and siltstone, as much as 1 m in diameter. There are no carbonate rinds on the clasts. There is no visible soil development.

Unit 3: 2.1-4.8 m. The unit is matrix supported and has a weak coarsening upward depositional sequence. The matrix is clay to fine, quartz-rich, subangular to subround sand, and effervesces when treated with HCl. However, there is no visible secondary carbonate. Clasts are angular to subangular, sandstone, mudstone, and siltstone as much as 1 m in diameter. There are no carbonate rinds on the clasts. There is no visible soil development.

Unit 4: 4.8 m and below. The unit has a weak coarsening upward depositional sequence. The matrix is clay to fine, quartz-rich, subangular to subround sand. Clasts are angular to subangular, sandstone, mudstone, and siltstone as much as 1.5 m in diameter. There is no visible secondary carbonate in the matrix and no carbonate rinds on clasts. However, the matrix effervesces when treated with HCl. There is no visible soil development. Only the uppermost 1 m of the unit is exposed. The lower portions of the unit are covered with colluvium. Bulk carbon and OSL samples SMCDOT 6 were taken 5.8 m below ground surface in sand and fine pebble material.

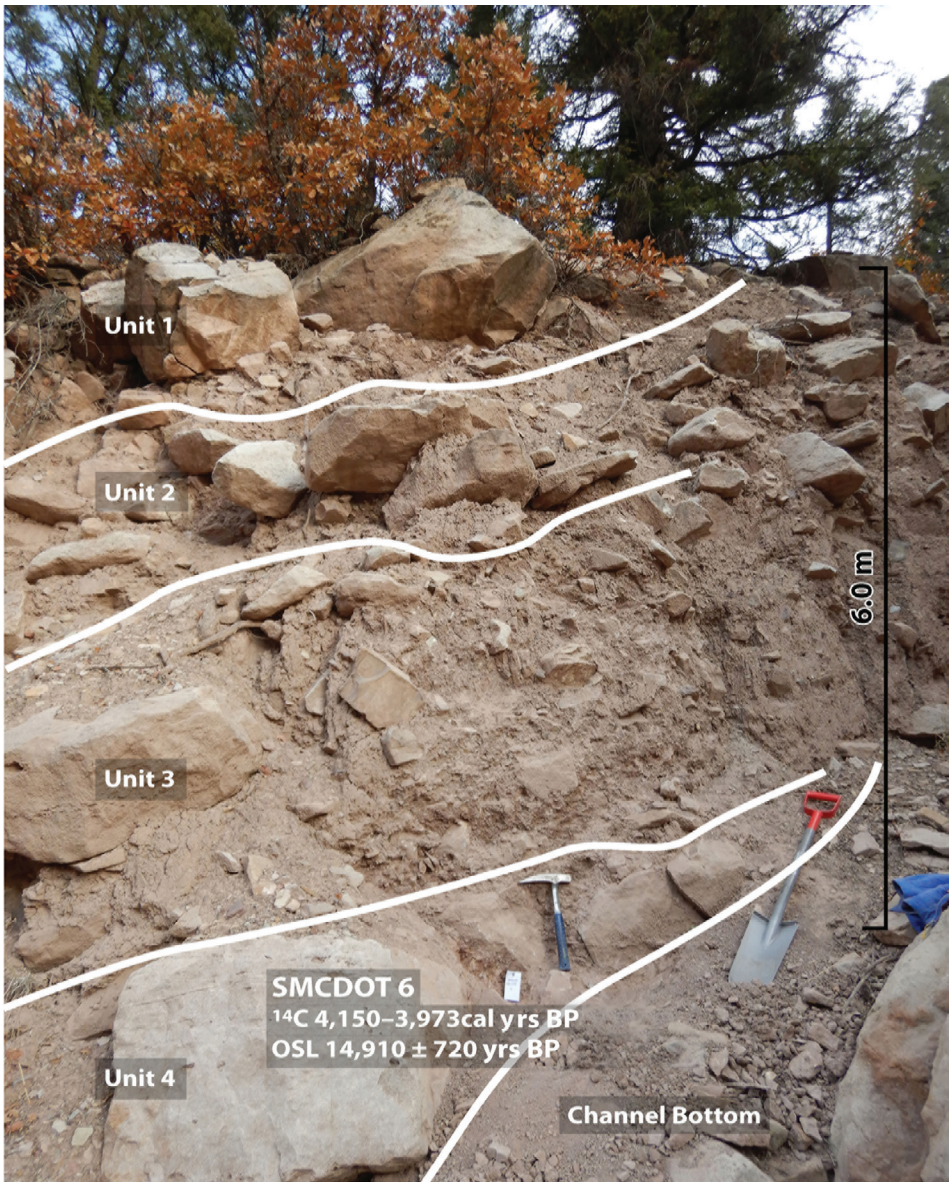

Figure B6. Fan B, SMCDOT 6. White lines represent approximate contacts between units. Sample SMCDOT 6 was taken approximately 5.8 m below ground surface (paper marker left of hammer). Bulk carbon analysis yielded an age estimate of 4,150-3,973 cal yrs BP. Optically stimulated luminescence analysis yielded an age estimate of 14,910 ± 720 yrs BP.

Figure B7 Profile description

Stratigraphy is not visible at this location. The unit is poorly sorted and clast supported. The matrix is clay to fine, quartz-rich, angular sand, with minor fine pebbles. Clasts are angular to subangular, sandstone and conglomerate as much as 1 m in diameter. There is no visible secondary carbonate development or other soil development. Bulk carbon and OSL samples SMCDOT 7 were taken 1.4 m bgs from a pocket of fine gravel and sand.

Figure B7. Fan B, SMCDOT 7. Individual units were more difficult to distinguish at this sample site given the channel geometry. A sample location was partially excavated from the channel side and sampled. Sample SMCDOT 7 was taken approximately 1.4 m below ground surface (paper marker). Bulk carbon analysis yielded an age estimate of 1,344-1,270 cal yrs BP.

APPENDIX C

Table C1. Radiocarbon dating by Beta Analytic, Inc., Miami, Florida. Samples SMCDOT 1-3 and 9-10 were taken from Fan A. Samples 4-7 were taken from Fan B. Depth BGS is Depth Below Ground Surface. Calibrated age are those discussed in the report. Sample SMCDOT 8 exceeded detectable limits because sample material analyzed by Beta Analytic may have been debris sourced from bedrock that resembled plant material.

Field Number	Latitude	Longitude	Laboratory Number	Depth BGS (m)	δ13C (‰)	^{14}C age (^{14}C yr BP) [a]	Calibrated Age (cal yr BP) [b]
SMCDOT C14 1	38.05977	-108.0287	Beta - 549468	1.5	-24.8	23,780 ± 80	28,011 – 27,660
SMCDOT C14 2	38.06008	-108.02863	Beta - 549469	0.76	-25.1	20,540 ± 70	25,051 – 24,425
SMCDOT C14 3	38.06062	-108.02876	Beta - 549470	0.7	-25.1	10,910 ± 30	12,819 – 12,707
SMCDOT C14 4	37.95710	-107.93747	Beta - 549471	4.6	-22.7	4,660 ± 30	5,468 – 5,314
SMCDOT C14 5	37.95718	-107.93745	Beta - 549472	3.5	-22.6	3,020 ± 30	3,271 – 3,140
SMCDOT C14 6	37.95716	-107.93785	Beta - 549473	5.8	-22.7	3,710 ± 30	4,150 – 3,973
SMCDOT C14 7	37.95720	-107.93749	Beta - 549474	1.4	-22.6	1,380 ± 30	1,344 – 1,270
SMCDOT C14 8	38.05977	-108.0287	Beta – 553468	0.4	-25.3	>43,500	–
SMCDOT C14 9	38.06008	-108.02863	Beta - 549475	0.15	-25	13,780 ± 40	16,905 – 16,432
SMCDOT C14 10	38.06062	-108.02876	Beta - 549476	0.4	-25	8,070 ± 30	9,037 – 8,971

a – Conventional radiocarbon age, normalized to -25‰, based on 5,568 year half-life; uncertainty ± 1 σ

b – Calibrated age calculated using INTCAL13 (Reimer and others, 2013); 0 yr B.P. = 1950 A.D.

Table C2. OSL dating by Steve Forman at the Baylor University Geoluminescence Dating Research Laboratory. Sample SMCDOT 3 was collected at Fan A. Samples SMCDOT 4 and 6 were collected at Fan B. Depth BGS is Depth Below Ground Surface. Significant variables are discussed in the report. Overdispersion values indicate age estimate yielded by OSL analysis are generally very reliable.

Field Number	Latitude	Longitude	Depth BGS (m)	Aliquots [a]	Equivalent Dose (De) (Gy)[b]	Over-dispersion (%)[c]	U (ppm) [d]	Th (ppm)[d]
SMCDOT 3	38.06062	-108.02876	0.7	40/40	7.42 ± 0.76	28± 3	3.09 ± 0.01	12.05 ± 0.01
SMCDOT 4	37.95710	-107.93747	4.6	35/41	39.93 ± 1.18	13± 2	1.62 ± 0.01	8.75 ± 0.01
SMCDOT 6	37.95716	-108.93785	6.2	34/46	50.02 ± 1.89	19± 2	2.06 ± 0.01	10.05 ± 0.01

Field Number	K_20(%)[d]	H_20 (%)	Cosmic Dose Rate (mGray/yr)	Dose Rate (mGray/yr)	SAR-OSL age(yr)[f]
SMCDOT 3	2.48 ± 0.01	5± 2	0.32 ± 0.032	3.72 ± 0.09	1,985 ± 210
SMCDOT 4	3.01 ± 0.01	15± 3	0.20 ± 0.023	3.24 ± 0.10	12,312 ±530
SMCDOT 6	3.13 ± 0.01	15±3	0.17 ± 0.017	3.36 ± 0.10	14,910 ± 720

a – Aliquots measured, used to define De population by Central or Minimum age models (Galbraith and Roberts, 2012).

b – Equivalent does calculated on a pure quartz fraction with ultra-small aliquots with 20-89 grains/aliquot and analyzed

under blue-light excitation (470 ± 20 mm) by Single Aliquot Regeneration protocols (SAR; Murray and Wintle, 2003; Wintle and Murray, 2006). Equivalent dose (De) was calculated by Central or Minimum age models (Galbraith and Roberts, 2012).

c – Overdispersion values reflects precision beyond instrumental errors; values of ≤ 20% (at 1 sigma limit) indicate low dispersion in equivalent does values and defines a unimodal distribution. Values > 20% are associated with mixed equivalent dose signature reflection multiple grain populations or partial solar resetting.

d– U, Th, Rb, and K content analyzed by inductively-coupled plasma-mass spectrometry by ALS Laboratories, Reno, NV; and includes dose contributions from Rb.